

Mechanics of moving contacts involving functionally graded multiferroics

S. E. TOKTAŞ, S. DAG

*Department of Mechanical Engineering, Middle East Technical University, Ankara 06800, Turkey,
e-mails: stoktas@metu.edu.tr, sdag@metu.edu.tr (corresponding author)*

THIS ARTICLE INTRODUCES SOLUTION PROCEDURES for moving contacts involving functionally graded multiferroic coatings. A moving rigid punch of a flat or a triangular profile is assumed to be in contact with a multi-layer medium comprising magneto-electro-elastic coating layers, elastic interlayers, and an elastic substrate, that is modelled as a half-plane. The formulation is based on wave equations of plane elastodynamics and Maxwell's equations. Applying Fourier and Galilean transformations, a singular integral equation of the second kind is derived for each of the flat and triangular punch problems. An expansion-collocation technique utilizing Jacobi polynomials is developed to numerically solve the integral equations. Proposed procedures are verified through comparisons to the results available in the literature. Parametric analyses carried out considering functionally graded magneto-electro-elastic coatings demonstrate the effects of the property variation profile, punch speed, and coating thickness on contact stresses, electric displacement, and magnetic induction. The methods presented could be of use in analysis and design studies of multiferroic layered systems subjected to moving contacts.

Key words: multiferroics, functionally graded materials, magneto-electro-elastic coatings, moving contacts, singular integral equations.



Copyright © 2023 The Authors.

Published by IPPT PAN. This is an open access article under the Creative Commons Attribution License CC BY 4.0 (<https://creativecommons.org/licenses/by/4.0/>).

1. Introduction

FERROIC MATERIALS ARE INTELLIGENT MATERIALS which are capable of exhibiting a phase transition around a critical temperature. This transition results in changes in the directional symmetry of the crystal structure and the physical characteristics. Primary ferroic materials consist of ferroelectrics, ferromagnetics, and ferroelastics. Spontaneous electric polarization in ferroelectrics, spin polarization in ferromagnetics, and strain in ferroelastics can be switched under the effect of electric field, magnetic field, and stress, respectively. All three primary ferroics display hysteresis behavior. Multiferroics – also known as magneto-electro-elastic (MEE) materials – possess two or more ferroic properties, which are coupled through magnetoelectric, piezoelectric, and magnetoelastic interactions. This phenomenon allows employment of the multiferroics in a broad range of

electronic devices. They can be found as single-phase compounds and multiphase materials, which include particulate composites, thin films, and composite laminates. Among the particular technological applications for which they are considered, one can mention transducers, sensors, memory devices, resonators, tunable devices, and oscillators [1–6].

A particular class of multiferroics that has attracted considerable research interest is that of functionally graded MEE surfaces and layers. Functionally graded materials (FGMs) are multiphase composites that have smooth spatial variations in the volume fractions of the constituent phases. Such variations result in an inhomogeneous macro-structure with spatially changing physical properties. Design, analysis, and testing of FGM structures have been conducted for a broad range of industries including aerospace, automotive, machinery and equipment, biomedical, energy, and electronics [7–11]. All physical properties in a functionally graded multiferroic layer are functions of the thickness coordinate, and the property variation profiles can be controlled by suitably specifying the volume fraction distributions of the constituent phases. Introduction of property gradations allows customization of the structural form, and this in turn facilitates optimization of elastic, magnetic, and electric responses under external effects. The prediction of these responses requires that the relevant physical properties be represented by continuous mathematical functions instead of constants [12–17].

The coupled magneto-electro-elastic behavior of multiferroics that are brought into contact with stationary or moving loading agents can be assessed by models based on contact mechanics. Such solutions allow calculation of singularities as well as stress, electric displacement, and magnetic induction distributions. For this reason, development of contact mechanics based procedures is among the main components of design studies involving such intelligent material systems. Contact mechanics analyses put forward for multiferroics consider elastostatic indentation and sliding contact, and elastodynamic moving contact problems. MEE half-planes and layers examined are assumed to be transversely isotropic with the symmetry axis normal to the contact area.

Solutions regarding elastostatic frictionless indentation are presented by CHEN *et al.* [18] and MA *et al.* [19] for a homogeneous and a functionally graded MEE half-plane, respectively. Most of the research work however seems to focus on elastostatic sliding frictional contact problems of multiferroics. ELLOUMI *et al.* [20, 21], ZHOU and KIM [22], and ZHOU and LEE [23] introduced closed form solutions for frictional contacts of homogeneous MEE half-planes. The sliding contact behavior of a functionally graded MEE half-plane is examined by ELLOUMI *et al.* [24]. Furthermore, elastostatic contact mechanics analyses for finite-thickness MEE coatings are performed by MA *et al.* [25], ZHANG *et al.* [26], and ZHANG *et al.* [27]. Lastly, ÇÖMEZ [28] and MA *et al.* [29] investigated the

effect of frictional heat generation on the contact response of a homogeneous and an FGM multiferroic layer, respectively. Except for the article by ZHANG *et al.* [27], which presents a multi-layer approach, in all studies on functionally graded magneto-electro-elastic materials, the material properties are represented by exponential functions that possess identical exponents. As a consequence, all property functions become proportional. Such an assumption is required to make the governing partial differential equations analytically tractable.

Analysis of moving contact problems of multiferroics requires that wave equations of elastodynamics be considered in the formulation. Adopting this approach, ÇÖMEZ [30] and ZHOU and LEE [31, 32] detailed solutions for a homogeneous MEE half-plane in contact with different types of moving rigid punches. It is demonstrated that coupled contact response resulting from a moving punch could be substantially different than that caused by a stationary punch. But, there is no prior work on moving contact problems of multi-layer or functionally graded MEE materials. ZHANG *et al.* [27] presented a general multi-layer approach for the sliding contact analysis of functionally graded magneto-electro-elastic materials. However, the formulation presented is based on the partial differential equations (PDE's) of elastostatics and not applicable for a moving punch problem for which the underlying theory is elastodynamics. Although elastostatic solutions are particularly useful for impending sliding motion of a punch, consideration of punch speed requires that PDEs of elastodynamics be included in the formulation.

Multiferroics have the potential to be employed in memory devices, sensors, and energy harvesters because of the stronger couplings observed among their magneto-electro-elastic fields [33–36]. In both multi-layer and functionally graded multiferroics, physical properties are functions of the thickness coordinate and the material is highly inhomogeneous. Homogeneous half-plane models do not suffice to realistically represent the moving contact behavior of such structural configurations. The main objective in the present study is therefore to develop general moving contact models for multi-layer and functionally graded multiferroics, that are based on the PDEs of plane elastodynamics.

The formulation is constructed by considering a multiferroic heterostructure consisting of an MEE coating, arbitrary number of elastic interlayers, and an elastic half-plane, which represents a substrate. The MEE coating is composed of N independently defined homogeneous sub-layers and in contact with a flat or a triangular rigid punch sliding with a velocity V . Through-the-thickness variations in the functionally graded MEE coatings are accounted for by specifying the physical properties of each sub-layer in accordance with the functions that define the spatial distributions. As a consequence, the property functions of the FGM coatings are not limited to proportional-exponential functions employed in previous studies on elastostatic contacts of graded magneto-electro-elastic me-

dia. In the solution procedure we present, realistic non-proportional property variations can be defined and implemented by using a sufficiently large value for the number of sub-layers, N .

By applying Fourier and Galilean transformations, the contact problem for each punch type is reduced to a singular integral equation of the second kind. Integral equations are converted to linear systems by expanding the primary unknowns into series of Jacobi polynomials and utilizing collocation points. The proposed procedure is verified by comparisons to the results available in the literature for homogeneous MEE materials. Number of sub-layers to be used to model the moving contact behavior of FGM MEE coatings is determined via convergence analysis. Presented numerical results illustrate the influences of property variation profile, punch speed, and coating thickness on contact stresses, stress intensity factors (SIFs), electric displacement, and magnetic induction.

The organization of the paper is as follows: Section 2 describes the formulation, and the derivation of general solutions. Section 3 presents the singular integral equations, and the numerical solution procedures. In Section 4, the results of the parametric analyses are provided, and Section 5 concludes the paper.

2. Formulation

The contact problems involving functionally graded multiferroics are depicted in Fig. 1. A flat or a triangular rigid moving punch of velocity V is in contact with a composite medium consisting of magneto-electro-elastic layers, purely elastic interlayers, and an elastic half-plane. The model is parametrically general in that the numbers of MEE layers and elastic interlayers are specified as N and M , respectively. The layers are numbered such that, $i = 1$, stands for the half-plane substrate; $i = 2, \dots, M + 1$, correspond to elastic interlayers; and $i = M + 2, \dots, N + M + 1$, represent the MEE layers. The problem is formulated within the confines of plane elastodynamics, i.e., the medium is in a state of either plane stress or strain. Normal and tangential forces transferred by the contact are respectively denoted by P and Q . Coulomb's friction law is assumed to hold, and the tangential force, Q , is specified as ηP , η being the coefficient of kinetic friction. The surface, $z = 0$ – including the contact zone – is electrically and magnetically insulated. Both the flat and the triangular punches, and the attached coordinate system X - Z move with a constant velocity V with respect to the fixed coordinate system x - z . The size of the contact zone is denoted by b , which is independent of P in the case of the flat punch problem. However, for the triangular profile, b is a function of P and the contact is incomplete.

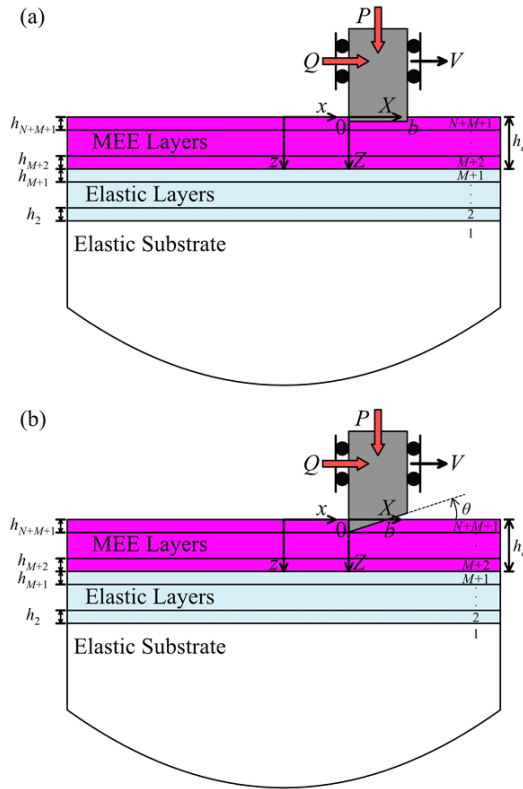


FIG. 1. Geometries of the moving contact problems considered: (a) flat punch problem; (b) triangular punch problem.

All layers and the half-plane are assumed to be transversely isotropic with z -axis as the axis of symmetry. The constitutive relations:

$$(2.1a) \quad \begin{Bmatrix} \sigma^{(i)}_{xx} \\ \sigma^{(i)}_{zz} \\ \sigma^{(i)}_{xz} \end{Bmatrix} = \begin{bmatrix} c^{(i)}_{11} & c^{(i)}_{13} & 0 \\ c^{(i)}_{13} & c^{(i)}_{33} & 0 \\ 0 & 0 & c^{(i)}_{44} \end{bmatrix} \begin{Bmatrix} \varepsilon^{(i)}_{xx} \\ \varepsilon^{(i)}_{zz} \\ 2\varepsilon^{(i)}_{xz} \end{Bmatrix}, \quad i = 1, \dots, M + 1,$$

$$(2.1b) \quad \begin{Bmatrix} \sigma^{(i)}_{xx} \\ \sigma^{(i)}_{zz} \\ \sigma^{(i)}_{xz} \end{Bmatrix} = \begin{bmatrix} c^{(i)}_{11} & c^{(i)}_{13} & 0 \\ c^{(i)}_{13} & c^{(i)}_{33} & 0 \\ 0 & 0 & c^{(i)}_{44} \end{bmatrix} \begin{Bmatrix} \varepsilon^{(i)}_{xx} \\ \varepsilon^{(i)}_{zz} \\ 2\varepsilon^{(i)}_{xz} \end{Bmatrix} - \begin{bmatrix} 0 & e^{(i)}_{31} \\ 0 & e^{(i)}_{33} \\ e^{(i)}_{15} & 0 \end{bmatrix} \begin{Bmatrix} E^{(i)}_x \\ E^{(i)}_z \end{Bmatrix} - \begin{bmatrix} 0 & f^{(i)}_{31} \\ 0 & f^{(i)}_{33} \\ f^{(i)}_{15} & 0 \end{bmatrix} \begin{Bmatrix} H^{(i)}_x \\ H^{(i)}_z \end{Bmatrix},$$

$i = M + 2, \dots, N + M + 1,$

$$(2.1c) \quad \begin{Bmatrix} D_{(i)x} \\ D_{(i)z} \end{Bmatrix} = \begin{bmatrix} 0 & 0 & e_{(i)15} \\ e_{(i)31} & e_{(i)33} & 0 \end{bmatrix} \begin{Bmatrix} \varepsilon_{(i)xx} \\ \varepsilon_{(i)zz} \\ 2\varepsilon_{(i)xz} \end{Bmatrix} \\ + \begin{bmatrix} \beta_{(i)11} & 0 \\ 0 & \beta_{(i)33} \end{bmatrix} \begin{Bmatrix} E_{(i)x} \\ E_{(i)z} \end{Bmatrix} + \begin{bmatrix} g_{(i)11} & 0 \\ 0 & g_{(i)33} \end{bmatrix} \begin{Bmatrix} H_{(i)x} \\ H_{(i)z} \end{Bmatrix}, \\ i = M + 2, \dots, N + M + 1,$$

$$(2.1d) \quad \begin{Bmatrix} B_{(i)x} \\ B_{(i)z} \end{Bmatrix} = \begin{bmatrix} 0 & 0 & f_{(i)15} \\ f_{(i)31} & f_{(i)33} & 0 \end{bmatrix} \begin{Bmatrix} \varepsilon_{(i)xx} \\ \varepsilon_{(i)zz} \\ 2\varepsilon_{(i)xz} \end{Bmatrix} \\ + \begin{bmatrix} g_{(i)11} & 0 \\ 0 & g_{(i)33} \end{bmatrix} \begin{Bmatrix} E_{(i)x} \\ E_{(i)z} \end{Bmatrix} + \begin{bmatrix} \mu_{(i)11} & 0 \\ 0 & \mu_{(i)33} \end{bmatrix} \begin{Bmatrix} H_{(i)x} \\ H_{(i)z} \end{Bmatrix}, \\ i = M + 2, \dots, N + M + 1,$$

are used in the formulation. A subscript in parentheses in the equations designates the layer number. The variables, $\sigma_{(i)jk}$, $\varepsilon_{(i)jk}$, $E_{(i)j}$, $H_{(i)j}$, $D_{(i)j}$, and $B_{(i)j}$, respectively denote stress, strain, electric field, magnetic field, electric displacement, and magnetic induction. Furthermore, the constants $c_{(i)jk}$, $e_{(i)jk}$, $f_{(i)jk}$, $g_{(i)jk}$, $\beta_{(i)jk}$, and $\mu_{(i)jk}$, stand for elastic, piezoelectric, piezomagnetic, and magnetolectric parameters, dielectric permittivities, and magnetic permeabilities. Strain, electric and magnetic fields are of the forms:

$$(2.2a) \quad \varepsilon_{(i)xx} = \frac{\partial u_{(i)}}{\partial x}, \quad \varepsilon_{(i)zz} = \frac{\partial w_{(i)}}{\partial z}, \quad \varepsilon_{(i)xz} = \frac{1}{2} \left(\frac{\partial u_{(i)}}{\partial z} + \frac{\partial w_{(i)}}{\partial x} \right), \\ i = 1, \dots, N + M + 1,$$

$$(2.2b) \quad E_{(i)x} = -\frac{\partial \phi_{(i)}}{\partial x}, \quad E_{(i)z} = -\frac{\partial \phi_{(i)}}{\partial z}, \quad H_{(i)x} = -\frac{\partial \psi_{(i)}}{\partial x}, \quad H_{(i)z} = -\frac{\partial \psi_{(i)}}{\partial z}, \\ i = M + 1, \dots, N + M + 1.$$

The functions $u_{(i)}$ and $w_{(i)}$ are displacement components in x - and z - directions; and $\phi_{(i)}$ and $\psi_{(i)}$ are electric and magnetic potentials.

Equations of motion in terms of stresses and displacements read:

$$(2.3) \quad \frac{\partial \sigma_{(i)xx}}{\partial x} + \frac{\partial \sigma_{(i)xz}}{\partial z} = \rho_{(i)} \frac{\partial^2 u_{(i)}}{\partial t^2}, \quad \frac{\partial \sigma_{(i)xz}}{\partial x} + \frac{\partial \sigma_{(i)zz}}{\partial z} = \rho_{(i)} \frac{\partial^2 w_{(i)}}{\partial t^2}, \\ i = 1, \dots, N + M + 1,$$

where $\rho_{(i)}$ is density and t is time. Electric displacement and magnetic induction components on the other hand, must satisfy Maxwell's equations:

$$(2.4) \quad \frac{\partial D_{(i)x}}{\partial x} + \frac{\partial D_{(i)z}}{\partial z} = 0, \quad \frac{\partial B_{(i)x}}{\partial x} + \frac{\partial B_{(i)z}}{\partial z} = 0, \quad i = M + 2, \dots, N + M + 1.$$

The governing partial differential equations are derived by substituting Eq. (2.1) into Eqs. (2.3) and (2.4), and using Eq. (2.2). The resulting PDE system is written as:

$$(2.5a) \quad c_{(i)11} \frac{\partial^2 u_{(i)}}{\partial x^2} + c_{(i)44} \frac{\partial^2 u_{(i)}}{\partial z^2} + (c_{(i)13} + c_{(i)44}) \frac{\partial^2 w_{(i)}}{\partial x \partial z} \\ = \rho_{(i)} \frac{\partial^2 u_{(i)}}{\partial t^2}, \quad i = 1, \dots, M + 1,$$

$$(2.5b) \quad (c_{(i)13} + c_{(i)44}) \frac{\partial^2 u_{(i)}}{\partial x \partial z} + c_{(i)44} \frac{\partial^2 w_{(i)}}{\partial x^2} + c_{(i)33} \frac{\partial^2 w_{(i)}}{\partial z^2} \\ = \rho_{(i)} \frac{\partial^2 w_{(i)}}{\partial t^2}, \quad i = 1, \dots, M + 1,$$

$$(2.5c) \quad c_{(i)11} \frac{\partial^2 u_{(i)}}{\partial x^2} + c_{(i)44} \frac{\partial^2 u_{(i)}}{\partial z^2} + (c_{(i)13} + c_{(i)44}) \frac{\partial^2 w_{(i)}}{\partial x \partial z} \\ + (e_{(i)15} + e_{(i)31}) \frac{\partial^2 \phi_{(i)}}{\partial x \partial z} + (f_{(i)15} + f_{(i)31}) \frac{\partial^2 \psi_{(i)}}{\partial x \partial z} = \rho_{(i)} \frac{\partial^2 u_{(i)}}{\partial t^2}, \\ i = M + 2, \dots, N + M + 1,$$

$$(2.5d) \quad (c_{(i)13} + c_{(i)44}) \frac{\partial^2 u_{(i)}}{\partial x \partial z} + c_{(i)44} \frac{\partial^2 w_{(i)}}{\partial x^2} + c_{(i)33} \frac{\partial^2 w_{(i)}}{\partial z^2} + e_{(i)15} \frac{\partial^2 \phi_{(i)}}{\partial x^2} \\ + e_{(i)33} \frac{\partial^2 \phi_{(i)}}{\partial z^2} + f_{(i)15} \frac{\partial^2 \psi_{(i)}}{\partial x^2} + f_{(i)33} \frac{\partial^2 \psi_{(i)}}{\partial z^2} = \rho_{(i)} \frac{\partial^2 w_{(i)}}{\partial t^2}, \\ i = M + 2, \dots, N + M + 1,$$

$$(2.5e) \quad (e_{(i)15} + e_{(i)31}) \frac{\partial^2 u_{(i)}}{\partial x \partial z} + e_{(i)15} \frac{\partial^2 w_{(i)}}{\partial x^2} + e_{(i)33} \frac{\partial^2 w_{(i)}}{\partial z^2} - \beta_{(i)11} \frac{\partial^2 \phi_{(i)}}{\partial x^2} \\ - \beta_{(i)33} \frac{\partial^2 \phi_{(i)}}{\partial z^2} - g_{(i)11} \frac{\partial^2 \psi_{(i)}}{\partial x^2} - g_{(i)33} \frac{\partial^2 \psi_{(i)}}{\partial z^2} = 0, \\ i = M + 2, \dots, N + M + 1,$$

$$(2.5f) \quad (f_{(i)15} + f_{(i)31}) \frac{\partial^2 u_{(i)}}{\partial x \partial z} + f_{(i)15} \frac{\partial^2 w_{(i)}}{\partial x^2} + f_{(i)33} \frac{\partial^2 w_{(i)}}{\partial z^2} - g_{(i)11} \frac{\partial^2 \phi_{(i)}}{\partial x^2} \\ - g_{(i)33} \frac{\partial^2 \phi_{(i)}}{\partial z^2} - \mu_{(i)11} \frac{\partial^2 \psi_{(i)}}{\partial x^2} - \mu_{(i)33} \frac{\partial^2 \psi_{(i)}}{\partial z^2} = 0, \\ i = M + 2, \dots, N + M + 1.$$

Note that unlike the PDEs of an elastostatic problem, right-hand-sides of the wave equations – which are given by Eqs. (2.5a)–(2.5d) – contain acceleration components. In order to eliminate time dependence, the Galilean transformation

$$(2.6) \quad x = X + Vt, \quad z = Z,$$

is introduced. For the steady-state motion of the punch, unknown functions can be expressed as follows:

$$\begin{aligned}
(2.7a) \quad & u_{(i)}(x, z, t) = U_{(i)}(X, Z), & i = 1, \dots, N + M + 1, \\
(2.7b) \quad & w_{(i)}(x, z, t) = W_{(i)}(X, Z), & i = 1, \dots, N + M + 1, \\
(2.7c) \quad & \phi_{(i)}(x, z, t) = \Phi_{(i)}(X, Z), & i = M + 2, \dots, N + M + 1, \\
(2.7d) \quad & \psi_{(i)}(x, z, t) = \Psi_{(i)}(X, Z), & i = M + 2, \dots, N + M + 1, \\
(2.7e) \quad & \sigma_{(i)xx}(x, z, t) = \sigma_{(i)XX}(X, Z), & i = 1, \dots, N + M + 1, \\
(2.7f) \quad & \sigma_{(i)zz}(x, z, t) = \sigma_{(i)ZZ}(X, Z), & i = 1, \dots, N + M + 1, \\
(2.7g) \quad & \sigma_{(i)xz}(x, z, t) = \sigma_{(i)XZ}(X, Z), & i = 1, \dots, N + M + 1, \\
(2.7h) \quad & D_{(i)x}(x, z, t) = D_{(i)X}(X, Z), & i = M + 2, \dots, N + M + 1, \\
(2.7i) \quad & D_{(i)z}(x, z, t) = D_{(i)Z}(X, Z), & i = M + 2, \dots, N + M + 1, \\
(2.7j) \quad & B_{(i)x}(x, z, t) = B_{(i)X}(X, Z), & i = M + 2, \dots, N + M + 1, \\
(2.7k) \quad & B_{(i)z}(x, z, t) = B_{(i)Z}(X, Z), & i = M + 2, \dots, N + M + 1.
\end{aligned}$$

The differential relations among the variables defined in the fixed and the moving coordinates are derived by applying chain rule. Considering $u_{(i)}(x, y, t)$ and its counterpart in the moving coordinate system, $U_{(i)}(X, Y)$, as representative functions, these relations are written as:

$$(2.8a) \quad \frac{\partial u_{(i)}}{\partial x} = \frac{\partial U_{(i)}}{\partial X}, \quad \frac{\partial^2 u_{(i)}}{\partial x^2} = \frac{\partial^2 U_{(i)}}{\partial X^2}, \quad \frac{\partial u_{(i)}}{\partial z} = \frac{\partial U_{(i)}}{\partial Z}, \quad \frac{\partial^2 u_{(i)}}{\partial z^2} = \frac{\partial^2 U_{(i)}}{\partial Z^2},$$

$$(2.8b) \quad \frac{\partial u_{(i)}}{\partial t} = -V \frac{\partial U_{(i)}}{\partial X}, \quad \frac{\partial^2 u_{(i)}}{\partial t^2} = V^2 \frac{\partial^2 U_{(i)}}{\partial X^2}.$$

Replacing the variables and differential operators in Eq. (2.5) with those defined in the moving system, we obtain:

$$(2.9a) \quad (c_{(i)11} - \lambda_{(i)}^2 c_{(i)44}) \frac{\partial^2 U_{(i)}}{\partial X^2} + c_{(i)44} \frac{\partial^2 U_{(i)}}{\partial Z^2} + (c_{(i)13} + c_{(i)44}) \frac{\partial^2 W_{(i)}}{\partial X \partial Z} = 0,$$

$$i = 1, \dots, M + 1,$$

$$(2.9b) \quad (c_{(i)13} + c_{(i)44}) \frac{\partial^2 U_{(i)}}{\partial X \partial Z} + c_{(i)44} (1 - \lambda_{(i)}^2) \frac{\partial^2 W_{(i)}}{\partial X^2} + c_{(i)33} \frac{\partial^2 W_{(i)}}{\partial Z^2} = 0,$$

$$i = 1, \dots, M + 1,$$

$$(2.9c) \quad (c_{(i)11} - \lambda_{(i)}^2 c_{(i)44}) \frac{\partial^2 U_{(i)}}{\partial X^2} + c_{(i)44} \frac{\partial^2 U_{(i)}}{\partial Z^2} + (c_{(i)13} + c_{(i)44}) \frac{\partial^2 W_{(i)}}{\partial X \partial Z}$$

$$+ (e_{(i)15} + e_{(i)31}) \frac{\partial^2 \Phi_{(i)}}{\partial X \partial Z} + (f_{(i)15} + f_{(i)31}) \frac{\partial^2 \Psi_{(i)}}{\partial X \partial Z} = 0,$$

$$i = M + 2, \dots, N + M + 1,$$

$$(2.9d) \quad (c_{(i)13} + c_{(i)44}) \frac{\partial^2 U_{(i)}}{\partial X \partial Z} + c_{(i)44} (1 - \lambda_{(i)}^2) \frac{\partial^2 W_{(i)}}{\partial X^2} + c_{(i)33} \frac{\partial^2 W_{(i)}}{\partial Z^2} \\ + e_{(i)15} \frac{\partial^2 \Phi_{(i)}}{\partial X^2} + e_{(i)33} \frac{\partial^2 \Phi_{(i)}}{\partial Z^2} + f_{(i)15} \frac{\partial^2 \Psi_{(i)}}{\partial X^2} + f_{(i)33} \frac{\partial^2 \Psi_{(i)}}{\partial Z^2} = 0, \\ i = M + 2, \dots, N + M + 1,$$

$$(2.9e) \quad (e_{(i)15} + e_{(i)31}) \frac{\partial^2 U_{(i)}}{\partial X \partial Z} + e_{(i)15} \frac{\partial^2 W_{(i)}}{\partial X^2} + e_{(i)33} \frac{\partial^2 W_{(i)}}{\partial Z^2} - \beta_{(i)11} \frac{\partial^2 \Phi_{(i)}}{\partial X^2} \\ - \beta_{(i)33} \frac{\partial^2 \Phi_{(i)}}{\partial Z^2} - g_{(i)11} \frac{\partial^2 \Psi_{(i)}}{\partial X^2} - g_{(i)33} \frac{\partial^2 \Psi_{(i)}}{\partial Z^2} = 0, \\ i = M + 2, \dots, N + M + 1,$$

$$(2.9f) \quad (f_{(i)15} + f_{(i)31}) \frac{\partial^2 U_{(i)}}{\partial X \partial Z} + f_{(i)15} \frac{\partial^2 W_{(i)}}{\partial X^2} + f_{(i)33} \frac{\partial^2 W_{(i)}}{\partial Z^2} - g_{(i)11} \frac{\partial^2 \Phi_{(i)}}{\partial X^2} \\ - g_{(i)33} \frac{\partial^2 \Phi_{(i)}}{\partial Z^2} - \mu_{(i)11} \frac{\partial^2 \Psi_{(i)}}{\partial X^2} - \mu_{(i)33} \frac{\partial^2 \Psi_{(i)}}{\partial Z^2} = 0, \\ i = M + 2, \dots, N + M + 1,$$

where $\lambda_{(i)}$ is dimensionless punch speed relative to layer i defined by

$$(2.10) \quad \lambda_{(i)} = \frac{V}{\sqrt{c_{(i)44}/\rho_{(i)}}}, \quad i = 1, \dots, N + M + 1.$$

The problems depicted in Fig. 1 are to be solved under continuity, boundary, and equilibrium conditions. Outside the contact zone, the surface, $Z = 0$, is stress-free, and in the contact region normal stress is unknown and shear stress is given by Coulomb's law. Furthermore, the surface is assumed to be electromagnetically insulated. These conditions are expressed as follows:

$$(2.11a) \quad \sigma_{(N+M+1)ZZ}(X, 0) = \begin{cases} S(X), & 0 < X < b, \\ 0, & X < 0, b < X, \end{cases}$$

$$(2.11b) \quad \sigma_{(N+M+1)XZ}(X, 0) = \begin{cases} \eta S(X), & 0 < X < b, \\ 0, & X < 0, b < X, \end{cases}$$

$$(2.11c) \quad D_{(N+M+1)Z}(X, 0) = 0, \quad B_{(N+M+1)Z}(X, 0) = 0, \quad -\infty < X < \infty.$$

The function, $S(X)$, in Eq. (2.11a, b) designates the unknown contact stress. Continuity requirements at the interfaces are of the forms:

$$(2.12a) \quad U_{(i)}(X, d_{(i)}) = U_{(i+1)}(X, d_{(i)}), \quad i = 1, \dots, N + M, \quad -\infty < X < \infty,$$

$$(2.12b) \quad W_{(i)}(X, d_{(i)}) = W_{(i+1)}(X, d_{(i)}), \quad i = 1, \dots, N + M, \quad -\infty < X < \infty,$$

$$(2.12c) \quad \sigma_{(i)ZZ}(X, d_{(i)}) = \sigma_{(i+1)ZZ}(X, d_{(i)}), \quad i = 1, \dots, N + M, \quad -\infty < X < \infty,$$

$$(2.12d) \quad \sigma_{(i)XZ}(X, d_{(i)}) = \sigma_{(i+1)XZ}(X, d_{(i)}),$$

$$i = 1, \dots, N+M, \quad -\infty < X < \infty,$$

$$(2.12e) \quad \Phi_{(i)}(X, d_{(i)}) = \Phi_{(i+1)}(X, d_{(i)}),$$

$$i = M+2, \dots, N+M, \quad -\infty < X < \infty,$$

$$(2.12f) \quad \Psi_{(i)}(X, d_{(i)}) = \Psi_{(i+1)}(X, d_{(i)}),$$

$$i = M+2, \dots, N+M, \quad -\infty < X < \infty,$$

$$(2.12g) \quad D_{(i)Z}(X, d_{(i)}) = D_{(i+1)Z}(X, d_{(i)}),$$

$$i = M+2, \dots, N+M, \quad -\infty < X < \infty,$$

$$(2.12h) \quad B_{(i)Z}(X, d_{(i)}) = B_{(i+1)Z}(X, d_{(i)}),$$

$$i = M+2, \dots, N+M, \quad -\infty < X < \infty,$$

where

$$(2.13) \quad d_{(i)} = \sum_{j=i+1}^{N+M+1} h_j,$$

are the Z -coordinates of the interfaces. Elastic interlayers do not display electro-magnetic behavior. For this reason, electric displacement and magnetic induction have to be zero at the interface, $Z = h_c$, which implies

$$(2.14) \quad D_{(M+2)Z}(X, h_c) = 0, \quad B_{(M+2)Z}(X, h_c) = 0, \quad -\infty < X < \infty.$$

The displacement derivative in the contact area is prescribed in accordance with the punch profile, and the punch itself is in equilibrium. The equalities:

$$(2.15a) \quad \frac{\partial W_{(N+M+1)}(X, 0)}{\partial X}$$

$$= \begin{cases} 0 & \text{for the flat punch,} \\ -\tan(\theta) & \text{for the triangular punch,} \end{cases} \quad 0 < X < b,$$

$$(2.15b) \quad \int_0^b S(t) dt = -P,$$

represent these two conditions. Additionally, regularity conditions require that all field quantities be bounded as $\sqrt{X^2 + Z^2} \rightarrow \infty$.

Applying the Fourier transformation in X -direction to the governing PDEs given by Eq. (2.9), the general solutions:

$$(2.16a) \quad U_{(i)}(X, Z) = \frac{1}{2\pi} \int_{-\infty}^{\infty} \sum_{j=1}^k G_{(i)j} e^{(s_{(i)j}Z + I\zeta X)} d\zeta, \quad -\infty < X < \infty,$$

$$i = 1, k = 2, \quad i = 2, \dots, M+1, k = 4, \quad i = M+2, \dots, N+M+1, k = 8,$$

$$(2.16b) \quad W_{(i)}(X, Z) = \frac{1}{2\pi} \int_{-\infty}^{\infty} \sum_{j=1}^k G_{(i)j} F_{(i)j} e^{(s_{(i)j}Z + I\zeta X)} d\zeta, \quad -\infty < X < \infty,$$

$$i = 1, k = 2, \quad i = 2, \dots, M + 1, k = 4, \quad i = M + 2, \dots, N + M + 1, k = 8,$$

$$(2.16c) \quad \Phi_{(i)}(X, Z) = \frac{1}{2\pi} \int_{-\infty}^{\infty} \sum_{j=1}^k G_{(i)j} R_{(i)j} e^{(s_{(i)j}Z + I\zeta X)} d\zeta, \quad -\infty < X < \infty,$$

$$i = M + 2, \dots, N + M + 1, k = 8,$$

$$(2.16d) \quad \Psi_{(i)}(X, Z) = \frac{1}{2\pi} \int_{-\infty}^{\infty} \sum_{j=1}^k G_{(i)j} Y_{(i)j} e^{(s_{(i)j}Z + I\zeta X)} d\zeta, \quad -\infty < X < \infty,$$

$$i = M + 2, \dots, N + M + 1, k = 8,$$

are derived. In these expressions, $s_{(i)j}$, is the j^{th} root of the characteristic equation of layer i , I is the imaginary unit, and $G_{(i)j}$ are unknown functions. The roots for $i = 1, \dots, M + 1$, are written as:

$$(2.17a) \quad s_{(1)1} = -\frac{\sqrt{2} \sqrt{\phi_{(1)1} + \sqrt{\phi_{(1)2}}}}{2 \phi_{(1)3}} |\zeta|, \quad s_{(1)2} = -\frac{\sqrt{2} \sqrt{\phi_{(1)1} - \sqrt{\phi_{(1)2}}}}{2 \phi_{(1)3}} |\zeta|,$$

$$\operatorname{Re}(s_{(1)1}) < 0, \quad \operatorname{Re}(s_{(1)2}) < 0,$$

$$(2.17b) \quad s_{(i)1} = \frac{\sqrt{2} \sqrt{\phi_{(i)1} + \sqrt{\phi_{(i)2}}}}{2 \phi_{(i)3}} |\zeta|, \quad s_{(i)2} = -\frac{\sqrt{2} \sqrt{\phi_{(i)1} + \sqrt{\phi_{(i)2}}}}{2 \phi_{(i)3}} |\zeta|,$$

$$i = 2, \dots, M + 1,$$

$$(2.17c) \quad s_{(i)3} = \frac{\sqrt{2} \sqrt{\phi_{(i)1} - \sqrt{\phi_{(i)2}}}}{2 \phi_{(i)3}} |\zeta|, \quad s_{(i)4} = -\frac{\sqrt{2} \sqrt{\phi_{(i)1} - \sqrt{\phi_{(i)2}}}}{2 \phi_{(i)3}} |\zeta|,$$

$$i = 2, \dots, M + 1,$$

$$(2.17d) \quad \phi_{(i)1} = -\lambda_{(i)}^2 c_{(i)33} c_{(i)44} - \lambda_{(i)}^2 c_{(i)44}^2 + c_{(i)11} c_{(i)33} - c_{(i)13}^2 - 2c_{(i)13} c_{(i)44},$$

$$i = 1, \dots, M + 1,$$

$$(2.17e) \quad \begin{aligned} \phi_{(i)2} = & \lambda_{(i)}^4 c_{(i)33}^2 c_{(i)44}^2 - 2\lambda_{(i)}^4 c_{(i)33} c_{(i)44}^3 + \lambda_{(i)}^4 c_{(i)44}^4 \\ & - 2\lambda_{(i)}^2 c_{(i)11} c_{(i)33}^2 c_{(i)44} + 2\lambda_{(i)}^2 c_{(i)11} c_{(i)33} c_{(i)44}^2 + 4c_{(i)13}^2 c_{(i)44}^2 \\ & + 2\lambda_{(i)}^2 c_{(i)13}^2 c_{(i)33} c_{(i)44} + 2\lambda_{(i)}^2 c_{(i)13}^2 c_{(i)44}^2 \\ & + 4\lambda_{(i)}^2 c_{(i)13} c_{(i)33} c_{(i)44}^2 + 4\lambda_{(i)}^2 c_{(i)13} c_{(i)44}^3 + 4\lambda_{(i)}^2 c_{(i)33} c_{(i)44}^3 \\ & + c_{(i)11}^2 c_{(i)33}^2 - 2c_{(i)11} c_{(i)13}^2 c_{(i)33} - 4c_{(i)11} c_{(i)13} c_{(i)33} c_{(i)44} \\ & - 4c_{(i)11} c_{(i)33} c_{(i)44}^2 + c_{(i)13}^4 + 4c_{(i)13}^3 c_{(i)44}, \quad i = 1, \dots, M + 1, \end{aligned}$$

$$(2.17f) \quad \phi_{(i)3} = \sqrt{c_{(i)33} c_{(i)44}}, \quad i = 1, \dots, M + 1,$$

where Re denotes the real part. The roots for the half-plane given by Eq. (2.17a) have negative real parts due to the regularity conditions. For the MEE layers, for which $i = M + 2, \dots, N + M + 1$, the roots are evaluated by solving the equation:

(2.18)

$$\begin{vmatrix} -\zeta^2(c_{(i)11} - \lambda_{(i)}^2 c_{(i)44}) + s_{(i)}^2 c_{(i)44} & I\zeta s_{(i)}(c_{(i)13} + c_{(i)44}) & I\zeta s_{(i)}(e_{(i)15} + e_{(i)31}) & I\zeta s_{(i)}(f_{(i)15} + f_{(i)31}) \\ I\zeta s_{(i)}(c_{(i)13} + c_{(i)44}) & -\zeta^2 c_{(i)44}(1 - \lambda_{(i)}^2) + s_{(i)}^2 c_{(i)33} & -\zeta^2 e_{(i)15} + s_{(i)}^2 e_{(i)33} & -\zeta^2 f_{(i)15} + s_{(i)}^2 f_{(i)33} \\ I\zeta s_{(i)}(e_{(i)15} + e_{(i)31}) & -\zeta^2 e_{(i)15} + s_{(i)}^2 e_{(i)33} & \zeta^2 \beta_{(i)11} - s_{(i)}^2 \beta_{(i)33} & \zeta^2 g_{(i)11} - s_{(i)}^2 g_{(i)33} \\ I\zeta s_{(i)}(f_{(i)15} + f_{(i)31}) & -\zeta^2 f_{(i)15} + s_{(i)}^2 f_{(i)33} & \zeta^2 g_{(i)11} - s_{(i)}^2 g_{(i)33} & \zeta^2 \mu_{(i)11} - s_{(i)}^2 \mu_{(i)33} \end{vmatrix} = 0.$$

The functions, $F_{(i)j}$, $R_{(i)j}$, and $Y_{(i)j}$, are of the forms:

(2.19a)
$$F_{(1)j} = -\frac{I\zeta s_{(1)j}(c_{(1)13} + c_{(1)44})}{-\zeta^2 c_{(1)44}(1 - \lambda_{(1)}^2) + s_{(1)j}^2 c_{(1)33}}, \quad j = 1, 2,$$

(2.19b)
$$F_{(i)j} = -\frac{I\zeta s_{(i)j}(c_{(i)13} + c_{(i)44})}{-\zeta^2 c_{(i)44}(1 - \lambda_{(i)}^2) + s_{(i)j}^2 c_{(i)33}},$$

$$i = 2, \dots, M + 1, j = 1, \dots, 4,$$

(2.19c)
$$\begin{Bmatrix} F_{(i)j} \\ R_{(i)j} \\ Y_{(i)j} \end{Bmatrix} = -\begin{bmatrix} -\zeta^2 c_{(i)44}(1 - \lambda_{(i)}^2) + s_{(i)j}^2 c_{(i)33} & -\zeta^2 e_{(i)15} + s_{(i)j}^2 e_{(i)33} & -\zeta^2 f_{(i)15} + s_{(i)j}^2 f_{(i)33} \\ -\zeta^2 e_{(i)15} + s_{(i)j}^2 e_{(i)33} & \zeta^2 \beta_{(i)11} - s_{(i)j}^2 \beta_{(i)33} & \zeta^2 g_{(i)11} - s_{(i)j}^2 g_{(i)33} \\ -\zeta^2 f_{(i)15} + s_{(i)j}^2 f_{(i)33} & \zeta^2 g_{(i)11} - s_{(i)j}^2 g_{(i)33} & \zeta^2 \mu_{(i)11} - s_{(i)j}^2 \mu_{(i)33} \end{bmatrix}^{-1} \times \begin{Bmatrix} I\zeta s_{(i)j}(c_{(i)13} + c_{(i)44}) \\ I\zeta s_{(i)j}(e_{(i)15} + e_{(i)31}) \\ I\zeta s_{(i)j}(f_{(i)15} + f_{(i)31}) \end{Bmatrix},$$

$$i = M + 2, \dots, N + M + 1, j = 1, \dots, 8.$$

Note that there are a total of 2 roots for the elastic substrate, $i = 1$; 4 roots for each of the elastic layers, $i = 2, \dots, M + 1$; and 8 roots for each of the MEE layers, $i = M + 2, \dots, N + M + 1$. The number of unknown functions, $G_{(i)j}$, is $8N + 4M + 2$. These functions are determined by using the interface and boundary conditions given in Eqs. (2.11)–(2.14).

The integral equation for each of the flat and triangular punch problems is derived by imposing the displacement derivative condition expressed by Eq. (2.15a). After a rather lengthy procedure involving asymptotic analyses of the integrands of the Fredholm kernels; displacement derivative, normal stress in X -direction, electric displacement, and magnetic induction, at the surface of the uppermost layer, $i = N + M + 1$, i.e., at $Z = 0$, are obtained as follows:

$$(2.20a) \quad \frac{\partial W_{(N+M+1)}(X, 0)}{\partial X} = \frac{p_1}{\pi} \int_0^b \frac{S(\xi)}{\xi - X} d\xi + p_2 \eta S(X) + \frac{1}{\pi} \int_0^b [k_{11}(\xi, X) + \eta k_{12}(\xi, X)] S(\xi) d\xi, \\ -\infty < X < \infty,$$

$$(2.20b) \quad \sigma_{(N+M+1)XX}(X, 0) = \frac{p_3 p_{10} \eta}{\pi} \int_0^b \frac{S(\xi)}{\xi - X} d\xi + (p_9 + p_4 p_{10}) S(X) \\ + \frac{p_{10}}{\pi} \int_0^b [\eta k_{21}(\xi, X) + k_{22}(\xi, X)] S(\xi) d\xi, \quad -\infty < X < \infty,$$

$$(2.20c) \quad D_{(N+M+1)X}(X, 0) = -\frac{(p_{12} p_5 + p_{13} p_7)}{\pi} \int_0^b \frac{S(\xi)}{\xi - X} d\xi \\ + \eta (p_{11} - p_{12} p_6 - p_{13} p_8) S(X) \\ - \frac{p_{12}}{\pi} \int_0^b [k_{31}(\xi, X) + \eta k_{32}(\xi, X)] S(\xi) d\xi \\ - \frac{p_{13}}{\pi} \int_0^b [k_{41}(\xi, X) + \eta k_{42}(\xi, X)] S(\xi) d\xi, \quad -\infty < X < \infty,$$

$$(2.20d) \quad B_{(N+M+1)X}(X, 0) = -\frac{(p_{13} p_5 + p_{15} p_7)}{\pi} \int_0^b \frac{S(\xi)}{\xi - X} d\xi \\ + \eta (p_{14} - p_{13} p_6 - p_{15} p_8) S(X) \\ - \frac{p_{13}}{\pi} \int_0^b [k_{31}(\xi, X) + \eta k_{32}(\xi, X)] S(\xi) d\xi \\ - \frac{p_{15}}{\pi} \int_0^b [k_{41}(\xi, X) + \eta k_{42}(\xi, X)] S(\xi) d\xi, \quad -\infty < X < \infty,$$

where the Fredholm kernels, k_{ij} , are expressed as:

$$(2.21a) \quad k_{11}(\xi, X) = \int_0^\infty (h_{11}(\zeta) - p_1) \sin(\zeta(\xi - X)) d\zeta,$$

$$(2.21b) \quad k_{12}(\xi, X) = \int_0^\infty (h_{12}(\zeta) - p_2) \cos(\zeta(\xi - X)) d\zeta,$$

$$(2.21c) \quad k_{21}(\xi, X) = \int_0^{\infty} (h_{21}(\zeta) - p_3) \sin(\zeta(\xi - X)) d\zeta,$$

$$(2.21d) \quad k_{22}(\xi, X) = \int_0^{\infty} (h_{22}(\zeta) - p_4) \cos(\zeta(\xi - X)) d\zeta,$$

$$(2.21e) \quad k_{31}(\xi, X) = \int_0^{\infty} (h_{31}(\zeta) - p_5) \sin(\zeta(\xi - X)) d\zeta,$$

$$(2.21f) \quad k_{32}(\xi, X) = \int_0^{\infty} (h_{32}(\zeta) - p_6) \cos(\zeta(\xi - X)) d\zeta,$$

$$(2.21g) \quad k_{41}(\xi, X) = \int_0^{\infty} (h_{41}(\zeta) - p_7) \sin(\zeta(\xi - X)) d\zeta,$$

$$(2.21h) \quad k_{42}(\xi, X) = \int_0^{\infty} (h_{42}(\zeta) - p_8) \cos(\zeta(\xi - X)) d\zeta.$$

The integrand functions, h_{ij} , and the constants, p_i , $i = 9, \dots, 15$, are provided in the Appendix. The coefficients, p_i , $i = 1, \dots, 8$, are calculated by numerical asymptotic analyses of the integrands.

3. Integral equations and numerical solution procedures

In this section, we outline the numerical solution procedures for the flat and triangular punch problems depicted in Fig. 1. The singular integral equation for each case is derived by equating the displacement derivative given by Eq. (2.20a) to the derivative dictated by the rigid punch profile. An expansion-collocation technique in which the contact stress is expanded into a series of Jacobi polynomials is developed so as to compute the unknown quantities.

3.1. Flat punch

We first introduce the variables, r and s , and the substitutions:

$$(3.1a) \quad \xi = \frac{b}{2}r + \frac{b}{2}, \quad X = \frac{b}{2}s + \frac{b}{2}, \quad k_{ij}(\xi, X) = \frac{2}{b}K_{ij}(r, s),$$

$$i = 1, \dots, 4, j = 1, 2, 0 < (\xi, X) < b, -1 < (r, s) < 1,$$

$$(3.1b) \quad \frac{S(X)}{P/b} = \frac{S(\frac{b}{2}s + \frac{b}{2})}{P/b} = S_{ZZ}(s),$$

to be able to express the integral equation and the unknown functions in the dimensionless interval $(-1, 1)$. Such a mapping from $(0, b)$ to $(-1, 1)$ is required in the implementation of the expansion-collocation technique, in which the interval $(-1, 1)$ is the domain for both the weight function and the orthogonal polynomials.

The function $S_{ZZ}(s)$ in Eq. (3.1b) is the dimensionless contact stress. Considering the fact that the displacement derivative, $\partial W(X, 0)/\partial X$, is zero in the contact zone for the flat punch, and using Eq. (2.20a), the singular integral equation

$$(3.2) \quad \frac{p_1}{\pi} \int_{-1}^1 \frac{S_{ZZ}(r)}{r-s} dr + \eta p_2 S_{ZZ}(s) + \frac{1}{\pi} \int_{-1}^1 [K_{11}(r, s) + \eta K_{12}(r, s)] S_{ZZ}(r) dr = 0, \quad -1 < s < 1,$$

is obtained. Furthermore, from the punch equilibrium condition given by Eq. (2.15b), it follows that,

$$(3.3) \quad \int_{-1}^1 S_{ZZ}(r) dr = -2.$$

The unknown contact stress is expanded into a series,

$$(3.4a) \quad S_{ZZ}(s) = w(s) \sum_{n=0}^{\infty} A_n P_n^{(\alpha_1, \alpha_2)}(s), \quad -1 < s < 1,$$

$$(3.4b) \quad w(s) = (1-s)^{\alpha_1} (1+s)^{\alpha_2},$$

where $w(s)$ is the weight function; α_1 and α_2 are strengths of singularity at the ends; A_n 's are unknown coefficients of the expansion; and $P_n^{(\alpha_1, \alpha_2)}(s)$ is the Jacobi polynomial of order n . Applying the function-theoretic method [37], α_1 and α_2 are found as follows:

$$(3.5) \quad \alpha_1 = \frac{1}{\pi} \arccot \left(-\frac{\eta p_2}{p_1} \right), \quad \alpha_2 = \frac{1}{\pi} \arccot \left(\frac{\eta p_2}{p_1} \right).$$

For the flat punch, $-1 < (\alpha_1, \alpha_2) < 0$ and $\alpha_1 + \alpha_2 = -1$. Substitution of the series form into the integral equation and regularization of the singular integrals by means of the orthogonality properties of Jacobi polynomials leads to:

$$(3.6a) \quad \sum_{n=0}^{\infty} A_n \left\{ -\frac{p_1}{2 \sin(\pi \alpha_1)} P_{n-1}^{(-\alpha_1, -\alpha_2)}(s) + \frac{1}{\pi} [Z_{1n}(s) + Z_{2n}(s)] \right\} = 0, \quad -1 < s < 1,$$

$$(3.6b) \quad Z_{1n}(s) = \int_{-1}^1 K_{11}(r, s) w(r) P_n^{(\alpha_1, \alpha_2)}(r) dr,$$

$$(3.6c) \quad Z_{2n}(s) = \eta \int_{-1}^1 K_{12}(r, s) w(r) P_n^{(\alpha_1, \alpha_2)}(r) dr.$$

Using the equilibrium condition given by Eq. (3.3), A_0 is obtained in the following form

$$(3.7) \quad A_0 = -\frac{2 \sin(\pi(1 + \alpha_1))}{\pi}.$$

Truncation of the infinite series in Eq. (3.6a) at $n = N_t$ results in an $N_t \times N_t$ linear system, which is solved by the use of the collocation points

$$(3.8) \quad s_i = \cos\left(\frac{(2i-1)\pi}{2N_t}\right), \quad i = 1, \dots, N_t.$$

Once the singular integral equation is solved and expansion coefficients are determined, mode I stress intensity factors at ends of the flat punch and all field quantities can also be calculated. Mode I stress intensity factors are defined by:

$$(3.9a) \quad k_I(0) = \lim_{X \rightarrow 0} \frac{-\sigma_{(N+M+1)ZZ}(X, 0)}{2^{\alpha_1} X^{\alpha_2}},$$

$$(3.9b) \quad k_I(b) = \lim_{X \rightarrow b} \frac{-\sigma_{(N+M+1)ZZ}(X, 0)}{2^{\alpha_2} (b-X)^{\alpha_1}}.$$

Normalized SIFs are then written as

$$(3.10a) \quad K_I(-1) = \frac{(b/2)^{\alpha_2}}{2(P/b)} k_I(0) = -\frac{1}{2} \sum_{n=0}^{N_t} A_n P_n^{(\alpha_1, \alpha_2)}(-1),$$

$$(3.10b) \quad K_I(1) = \frac{(b/2)^{\alpha_1}}{2(P/b)} k_I(b) = -\frac{1}{2} \sum_{n=0}^{N_t} A_n P_n^{(\alpha_1, \alpha_2)}(1).$$

Dimensionless stress, electric displacement, and magnetic induction in X -direction are of the forms:

$$(3.11a) \quad S_{XX}(s) = \frac{\sigma_{(N+M+1)XX}(X, 0)}{P/b} \\ = \frac{p_3 p_{10} \eta}{\pi} \int_{-1}^1 \frac{S_{ZZ}(r)}{r-s} dr + (p_9 + p_4 p_{10}) S_{ZZ}(s) \\ + \frac{p_{10}}{\pi} \int_{-1}^1 [\eta K_{21}(r, s) + K_{22}(r, s)] S_{ZZ}(r) dr, \quad -\infty < s < \infty,$$

$$\begin{aligned}
(3.11b) \quad \Omega_X(s) &= \frac{D_{(N+M+1)X}(X, 0)}{P/(p_{16}b)} \\
&= -\frac{(p_{12}p_5 + p_{13}p_7)p_{16}}{\pi} \int_{-1}^1 \frac{S_{ZZ}(r)}{r-s} dr \\
&\quad + \eta p_{16}(p_{11} - p_{12}p_6 - p_{13}p_8)S_{ZZ}(s) \\
&\quad - \frac{p_{12}p_{16}}{\pi} \int_{-1}^1 [K_{31}(r, s) + \eta K_{32}(r, s)]S_{ZZ}(r) dr \\
&\quad - \frac{p_{13}p_{16}}{\pi} \int_{-1}^1 [K_{41}(r, s) + \eta K_{42}(r, s)]S_{ZZ}(r) dr, \quad -\infty < s < \infty,
\end{aligned}$$

$$\begin{aligned}
(3.11c) \quad \Gamma_X(s) &= \frac{B_{(N+M+1)X}(X, 0)}{P/(p_{17}b)} \\
&= -\frac{(p_{13}p_5 + p_{15}p_7)p_{17}}{\pi} \\
&\quad \times \int_{-1}^1 \frac{S_{ZZ}(r)}{r-s} dr + \eta p_{17}t(p_{14} - p_{13}p_6 - p_{15}p_8)S_{ZZ}(s) \\
&\quad - \frac{p_{13}p_{17}}{\pi} \int_{-1}^1 [K_{31}(r, s) + \eta K_{32}(r, s)]S_{ZZ}(r) dr \\
&\quad - \frac{p_{15}p_{17}}{\pi} \int_{-1}^1 [K_{41}(r, s) + \eta K_{42}(r, s)]S_{ZZ}(r) dr, \quad -\infty < s < \infty.
\end{aligned}$$

The constants p_{16} and p_{17} are provided in the Appendix.

3.2. Triangular punch

The moving triangular punch problem examined is shown in Fig. 1(b). The substitutions used are given by Eq. (3.1a). The normalized stress in this case is defined as

$$(3.12) \quad \frac{S(X)}{c_{44}(0) \tan(\theta)} = \frac{S(\frac{b}{2}s + \frac{b}{2})}{c_{44}(0) \tan(\theta)} = S_{ZZ}(s),$$

where $c_{44}(0)$ stands for the value of the shear modulus at $Z = 0$, and θ is the punch inclination angle. The singular integral equation and the complementary equilibrium condition then take the forms:

$$(3.13a) \quad \frac{p_1}{\pi} \int_{-1}^1 \frac{S_{ZZ}(r)}{r-s} dr + \eta p_2 S_{ZZ}(s) \\ + \frac{1}{\pi} \int_{-1}^1 [K_{11}(r,s) + \eta K_{12}(r,s)] S_{ZZ}(r) dr = -\frac{1}{c_{44}(0)}, \quad -1 < s < 1,$$

$$(3.13b) \quad \int_{-1}^1 S_{ZZ}(r) dr = -\frac{2P}{c_{44}(0) \tan(\theta)b}.$$

$S_{ZZ}(s)$ expression for the triangular punch is exactly the same as that given by Eq. (3.4). However, in this case, $0 < \alpha_1 < 1$, $-1 < \alpha_2 < 0$, and $\alpha_1 + \alpha_2 = 0$. Upon substituting the series representation of $S_{ZZ}(s)$ into Eq. (3.13a), the functional equation

$$(3.14) \quad \sum_{n=0}^{\infty} A_n \left\{ -\frac{p_1}{\sin(\pi\alpha_1)} P_n^{(-\alpha_1, -\alpha_2)}(s) + \frac{1}{\pi} [Z_{1n}(s) + Z_{2n}(s)] \right\} \\ = -\frac{1}{c_{44}(0)}, \quad -1 < s < 1,$$

is obtained. The integrals $Z_{1n}(s)$ and $Z_{2n}(s)$ are expressed by Eq. (3.6b). Truncating the infinite series at $n = N_t$, and using the collocation points

$$(3.15) \quad s_i = \cos\left(\frac{(2i-1)\pi}{2(N_t+1)}\right), \quad i = 1, \dots, N_t + 1,$$

an $(N_t + 1) \times (N_t + 1)$ system of linear equations is generated for the unknown coefficients. The required contact force is derived by considering Eq. (3.13b), and written as

$$(3.16) \quad \frac{P}{c_{44}(0) \tan(\theta)b} = \frac{A_0 \pi \alpha_1}{\sin(\pi(1 + \alpha_1))}.$$

Mode I stress intensity factor at the sharp end, $X = 0$, is defined by

$$(3.17) \quad k_I(0) = \lim_{X \rightarrow 0} (-X^{\alpha_1} \sigma_{(N+M+1)ZZ}(X, 0)),$$

which leads to

$$(3.18) \quad K_I(-1) = \frac{k_I(0)}{c_{44}(0) \tan(\theta)b^{\alpha_1}} = -\sum_{n=0}^{N_t} A_n P_n^{(\alpha_1, \alpha_2)}(-1).$$

The other functions representing the contact response of the multiferroic heterostructure, i.e., dimensionless stress, electric displacement, and magnetic induction in X -direction are expressed in dimensionless forms as follows:

$$\begin{aligned}
 (3.19a) \quad S_{XX}(s) &= \frac{\sigma_{(N+M+1)XX}(X, 0)}{c_{44}(0) \tan(\theta)} \\
 &= \frac{p_3 p_{10} \eta}{\pi} \int_{-1}^1 \frac{S_{ZZ}(r)}{r-s} dr + (p_9 + p_4 p_{10}) S_{ZZ}(s) \\
 &\quad + \frac{p_{10}}{\pi} \int_{-1}^1 [\eta K_{21}(r, s) + K_{22}(r, s)] S_{ZZ}(r) dr, \quad -\infty < s < \infty,
 \end{aligned}$$

$$\begin{aligned}
 (3.19b) \quad \Omega_X(s) &= \frac{D_{(N+M+1)X}(X, 0)}{c_{44}(0) \tan(\theta) / p_{16}} \\
 &= -\frac{(p_{12} p_5 + p_{13} p_7) p_{16}}{\pi} \int_{-1}^1 \frac{S_{ZZ}(r)}{r-s} dr \\
 &\quad + \eta p_{16} (p_{11} - p_{12} p_6 - p_{13} p_8) S_{ZZ}(s) \\
 &\quad - \frac{p_{12} p_{16}}{\pi} \int_{-1}^1 [K_{31}(r, s) + \eta K_{32}(r, s)] S_{ZZ}(r) dr \\
 &\quad - \frac{p_{13} p_{16}}{\pi} \int_{-1}^1 [K_{41}(r, s) + \eta K_{42}(r, s)] S_{ZZ}(r) dr, \quad -\infty < s < \infty,
 \end{aligned}$$

$$\begin{aligned}
 (3.19c) \quad \Gamma_X(s) &= \frac{B_{(N+M+1)X}(X, 0)}{c_{44}(0) \tan(\theta) / p_{17}} \\
 &= -\frac{(p_{13} p_5 + p_{15} p_7) p_{17}}{\pi} \int_{-1}^1 \frac{S_{ZZ}(r)}{r-s} dr \\
 &\quad + \eta p_{17} (p_{14} - p_{13} p_6 - p_{15} p_8) S_{ZZ}(s) \\
 &\quad - \frac{p_{13} p_{17}}{\pi} \int_{-1}^1 [K_{31}(r, s) + \eta K_{32}(r, s)] S_{ZZ}(r) dr \\
 &\quad - \frac{p_{15} p_{17}}{\pi} \int_{-1}^1 [K_{41}(r, s) + \eta K_{42}(r, s)] S_{ZZ}(r) dr, \quad -\infty < s < \infty.
 \end{aligned}$$

4. Numerical results

The contact problem geometries considered in the parametric analyses are shown in Fig. 1. A rigid punch of a flat or a triangular profile slides with a ve-

locity V over the surface of a multi-layer structure, which is in a state of plane strain. The FGM MEE coating is of thickness, h_c , and assumed to be 100% barium titanate (BaTiO_3) – cobalt ferrite (CoFe_2O_4) composite at $Z = 0$, and 100% lanthanum nickel oxide (LaNiO_3) at the interface $Z = h_c$. The volume fraction of each component in the barium titanate-cobalt ferrite composite is specified as 50%. Barium titanate acts as the piezoelectric constituent, whereas cobalt ferrite possesses magnetostrictive characteristics. The half-plane material is assumed to be silicon. The interlayers between the half-plane and the FGM MEE coating are yttria-stabilized zirconia (YSZ), ceric oxide (CeO_2), and LaNiO_3 , which are identified by the layer numbers $i = 2, 3$, and 4. M is therefore set as 3. The properties of all materials are provided in Table 1. Note that Silicon, YSZ, and CeO_2 are isotropic; LaNiO_3 is cubic; and the BaTiO_3 – CoFe_2O_4 composite is transversely isotropic. The FGM MEE coating is modelled by N homogeneous MEE layers, and the value of N is determined through convergence analysis as described in Section 4.2. The general configuration for the multi-layer system is discussed by SCIGAJ *et al.* [34].

Previous solutions on contact mechanics of functionally graded magneto-electro-elastic materials are developed for elastostatic loading. In most of the studies, the spatial variations are represented by proportional exponential functions. The exponents of the functions are taken equal to be able to formulate the problem in terms of the constant coefficient PDEs. The multi-layer modelling approach depicted in Fig. 1 however allows consideration of nonproportional spatial variations in all material properties. Additionally, the model is capable of accounting for the multi-layer configurations encountered in applications. Thus, the methods introduced allow accurate computation of contact stresses induced in multiferroic heterostructures due to moving contacts.

Through-the-thickness variation of any of the properties of the functionally graded MEE coating is expressed in terms of a power function in the form,

$$(4.1) \quad \chi(Z) = \chi_0 + (\chi_h - \chi_0)(Z/h_c)^\gamma, \quad 0 < Z < h_c,$$

where χ is a generic property, h_c is the thickness of the coating, the subscripts 0 and h , respectively, indicate properties computed at $Z = 0$ and h_c , and γ is the power function exponent. Note that at the interface, $Z = h_c$, χ is equal to χ_h , which designates the generic property of LaNiO_3 . The power function representation assures the continuity of all required parameters at the interface. Since LaNiO_3 does not display multiferroic behavior, its electromagnetic properties are all zero. Thus, the electromagnetic properties of the MEE coating are also zero at $Z = h_c$.

Material parameters of each layer in the FGM MEE coating are computed at the centroid in accordance with the general through-the-thickness variations specified by Eq. (4.1). In parametric analyses, we consider three different FGM

TABLE 1. Material properties used in the parametric analyses [32, 38–43].

Property	Silicon	YSZ	CeO ₂	LaNiO ₃	BaTiO ₃ -CoFe ₂ O ₄
c_{11} [GPa]	188.37	284.14	286.93	405.5	226
c_{13} [GPa]	53.13	127.66	128.91	119.2	124
c_{33} [GPa]	188.37	284.14	286.93	405.5	216
c_{44} [GPa]	67.62	78.24	79.01	103.6	44
e_{15} [C/m ²]					5.8
e_{31} [C/m ²]					-2.2
e_{33} [C/m ²]					9.3
f_{15} [N/Am]					275
f_{31} [N/Am]					290.2
f_{33} [N/Am]					350
β_{11} [10^{-9} C ² /Nm ²]					5.64
β_{33} [10^{-9} C ² /Nm ²]					6.35
μ_{11} [10^{-6} Ns ² /C ²]					297
μ_{33} [10^{-6} Ns ² /C ²]					83.5
ρ [kg/m ³]	2330	6090	7215	7200	5550
g_{11} [10^{-12} Ns/VC]					5.367
g_{33} [10^{-12} Ns/VC]					2737.5

TABLE 2. Exponent values used in the parametric analyses.

Property	Exponent	FGM1	FGM2	FGM3
c_{11}	γ_1	1	1.5	3.0
c_{13}	γ_2	1	1.5	3.0
c_{33}	γ_3	1	1.5	3.0
c_{44}	γ_4	1	1.5	3.0
e_{15}	γ_5	1	1.5	3.0
e_{31}	γ_6	1	1.5	3.0
e_{33}	γ_7	1	1.5	3.0
f_{15}	γ_8	1	1.6	3.2
f_{31}	γ_9	1	1.6	3.2
f_{33}	γ_{10}	1	1.6	3.2
β_{11}	γ_{11}	1	1.6	3.2
β_{33}	γ_{12}	1	1.6	3.2
μ_{11}	γ_{13}	1	1.8	3.6
μ_{33}	γ_{14}	1	1.8	3.6
ρ	γ_{15}	1	2.0	4.0
g_{11}	γ_{16}	1	2.0	4.0
g_{33}	γ_{17}	1	2.0	4.0

coatings (FGM1, FGM2, FGM3) and a homogeneous coating (H). Table 2 tabulates the exponents of the power functions for FGMs and their numerical values. FGM1 is the linear variation coating for which all exponents are unity. FGM2 and FGM3 are barium titanate – cobalt ferrite rich and their exponents are greater than one. The parameters of the homogeneous MEE coating, H, are equal to those of the barium titanate – cobalt ferrite composite given in Table 1.

4.1. Verification

Developed procedures are verified by comparisons to the numerical results provided by ZHOU and LEE [32]. The problem solved in [32] is that of a homogeneous magneto-electro-elastic half-plane in contact with a frictionless moving flat punch of velocity V , which can be defined as a special case of the general problem depicted in Fig. 1(a). The half-plane is assumed to be a barium titanate (BaTiO_3) – cobalt ferrite (CoFe_2O_4) composite, and in a state of plane strain. Homogenized properties of the MEE half-plane are the same as those of the barium titanate – cobalt ferrite composite provided in Table 1. The model depicted in Fig. 1(a) allows the calculation of the contact stresses for the homogeneous half-plane, provided that a single homogeneous MEE layer with a sufficiently large thickness, h_c , is considered. For this reason, in the computations, N and M are respectively assigned the values 1 and 3, and the relative thickness, h_c/b , is set as 10.

Figure 2 shows comparisons of the contact stresses for a frictionless flat punch computed by considering four different values of λ , which is the dimensionless punch velocity relative to the homogeneous MEE half-plane and defined by

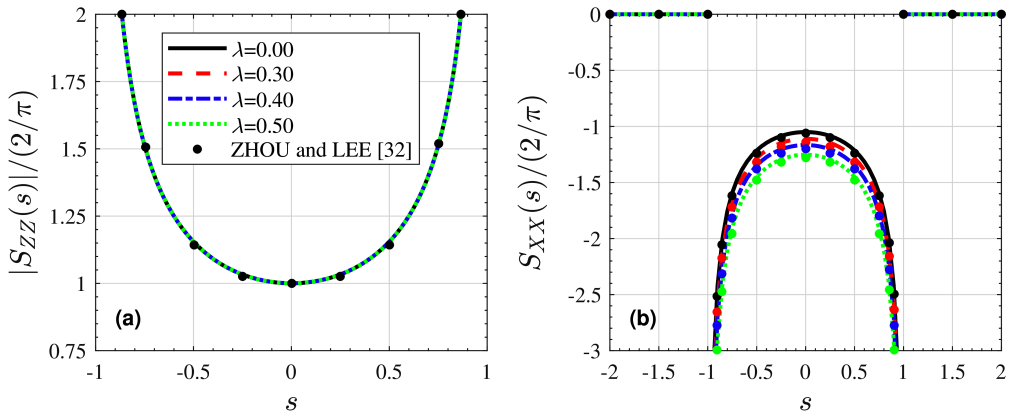


FIG. 2. Comparisons of contact stresses for an MEE half-plane loaded by the moving flat punch: (a) normal stress; (b) normal stress in X-direction. $\eta = 0$, $h_2/b = 0.5$, $h_3/b = 0.25$, $h_4/b = 0.4375$, $h_c/b = 10$.

$$(4.2) \quad \lambda = \frac{V}{\sqrt{c_{44}/\rho}},$$

where c_{44} and ρ are shear modulus and density of barium titanate-cobalt ferrite composite. Normalized contact stresses, $|S_{ZZ}(s)|/(2/\pi)$ and $S_{XX}(s)/(2/\pi)$, are plotted for four different values of the dimensionless punch velocity. Note that normalized contact stress, $S_{ZZ}(s)$, is always negative whereas $S_{XX}(s)$ takes on positive and negative values. In order to be able more clearly illustrate the variations in the magnitude of $S_{ZZ}(s)$, its absolute value is plotted in all figures. The function $S_{XX}(s)$ itself is plotted so as to present the changes in its sign.

ZHOU and LEE [32] based the formulation of the frictionless moving contact problem on the elastodynamic theory. The contact stresses we generated are in excellent agreement with their results, which is a verification of the developed procedures. Both findings indicate that normalized contact stress, $S_{ZZ}(s)/(2/\pi)$, is the same for elastostatic and elastodynamic cases. This stress is not affected by the dimensionless punch velocity, λ . Furthermore, dimensionless normal stress in X -direction, $S_{XX}(s)/(2/\pi)$, is zero outside the contact zone for all λ values. Within the contact zone however, λ has an impact on the variation of $S_{XX}(s)/(2/\pi)$, and there are differences between elastostatic and elastodynamic results. Although $S_{ZZ}(s)/(2\pi)$ is independent of the punch velocity for the homogeneous MEE half-plane problem considered, our parametric analyses presented in Sections 4.3 and 4.4 indicate that in the case of moving contacts of FGM MEE coatings, both contact stresses are functions of the punch velocity.

4.2. Convergence analysis

A convergence analysis is carried out to determine the number of layers, N , to be used in the modelling of FGM multiferroic coatings. The configuration defined for the moving flat punch, depicted in Fig. 1(a), is considered for this purpose. The analysis is performed for the MEE coating FGM2; and kinetic friction coefficient, η , and relative punch speed, $\lambda_{(1)}$, are both set as 0.3. The results are provided in Table 3. Normalized contact stresses, S_{ZZ} and S_{XX} , and

TABLE 3. Number of layers, stresses, electric displacement, magnetic induction and percent approximate error computed at $s = 0$ for the FGM2 coating loaded by the moving flat punch.

$h_2/b = 0.5$, $h_3/b = 0.25$, $h_4/b = 0.4375$, $h_c/b = 1$, $\eta = 0.3$, $\lambda_{(1)} = 0.3$.

N	$S_{ZZ}(0)$	ε_a	$S_{XX}(0)$	ε_a	$\Omega_X(0)$	ε_a	$\Gamma_X(0)$	ε_a
10	-0.7272	-	-0.7611	-	-0.1834	-	-0.3901	-
50	-0.7276	0.05	-0.7588	0.30	-0.1934	5.17	-0.4036	3.34
100	-0.7277	0.01	-0.7587	0.01	-0.1941	0.36	-0.4045	0.22
150	-0.7277	0.00	-0.7587	0.00	-0.1943	0.10	-0.4047	0.05

electric displacement and magnetic induction in X -direction, Ω_X and Γ_X , at the mid-point of the contact zone $s = 0$, and respective percent approximate errors are computed by successively increasing the number of layers, N . The percent approximate error, ε_a , is defined by

$$(4.3) \quad \varepsilon_a = \left| \frac{\text{current value} - \text{previous value}}{\text{current value}} \right| \times 100.$$

The approximate error drops significantly as the number of layers is increased, and all percent errors are less than 0.5% for $N = 100$. This value is thus used in the parametric analyses.

4.3. Flat punch

The results generated for a flat punch in moving contact with a multiferroic heterostructure are provided in Figs. 3–8 and Tables 4–6. The problem definition is depicted in Fig. 1(a). Figures 3 and 4 present the numerical results calculated for four different types of magneto-electro-elastic coatings, which are FGM1, FGM2, FGM3, and H. The dimensionless punch speed, $\lambda_{(1)}$, and the friction coefficient are both 0.3. Figure 3(a) shows that in the central region of the contact zone, magnitude of the contact stress, S_{ZZ} , computed for the homogeneous MEE coating is smaller than those evaluated for the FGM coatings. The results given in Table 4 however point out that stress intensity factors at the end points, $K_I(-1)$ and $K_I(1)$, are larger for the homogeneous MEE coating. Lowest stress intensity values are evaluated for the linear variation coating FGM1. Figure 3(b) displays the normalized contact stress in X -direction, S_{XX} , which is known to possess a strong influence on the crack formation behavior at the surface. The tensile

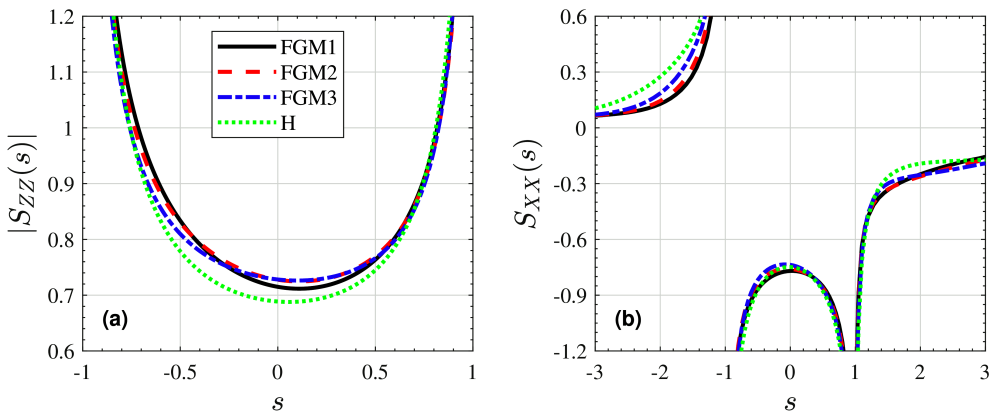


FIG. 3. Normalized contact stresses computed for different MEE coatings loaded by the moving flat punch: (a) normal stress; (b) normal stress in X -direction. $h_2/b = 0.5$, $h_3/b = 0.25$, $h_4/b = 0.4375$, $h_c/b = 1$, $\eta = 0.3$, $\lambda_{(1)} = 0.3$.

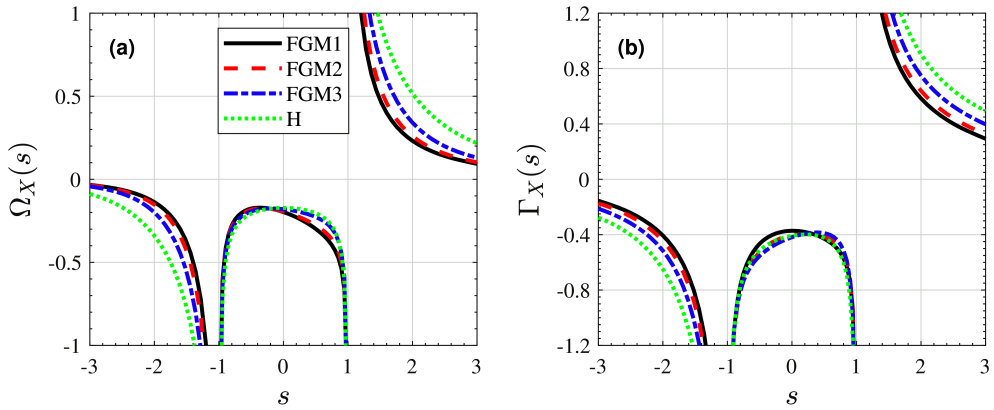


FIG. 4. Normalized electric displacement and magnetic induction computed for different MEE coatings loaded by the moving flat punch: (a) electric displacement; (b) magnetic induction. $h_2/b = 0.5$, $h_3/b = 0.25$, $h_4/b = 0.4375$, $h_c/b = 1$, $\eta = 0.3$, $\lambda_{(1)} = 0.3$.

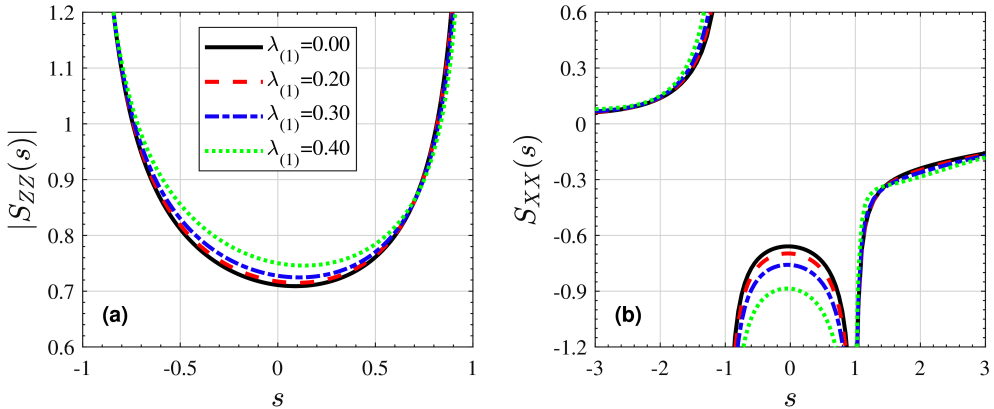


FIG. 5. Normalized contact stresses as functions of $\lambda_{(1)}$ computed for the FGM2 coating loaded by the moving flat punch: (a) normal stress; (b) normal stress in X -direction. $h_2/b = 0.5$, $h_3/b = 0.25$, $h_4/b = 0.4375$, $h_c/b = 1$, $\eta = 0.3$.

stress generated in the wake of the contact zone near $s = -1$, is largest in the homogeneous coating and smallest in FGM1. The effect of coating type on the normalized electric displacement and the magnetic induction in X -direction, i.e., on Ω_X and Γ_X , is examined in Fig. 4. For $|s| > 1$, the largest electric displacement and magnetic induction magnitudes are generated in the homogeneous coating. The linear variation coating FGM1 again leads to lowest magnitudes.

The impact of the dimensionless punch speed, $\lambda_{(1)}$, is illustrated in Figs. 5 and 6 and Table 5. Figure 5 shows that in the neighborhood of the mid-point of the contact zone, magnitudes of both of the normalized contact stresses,

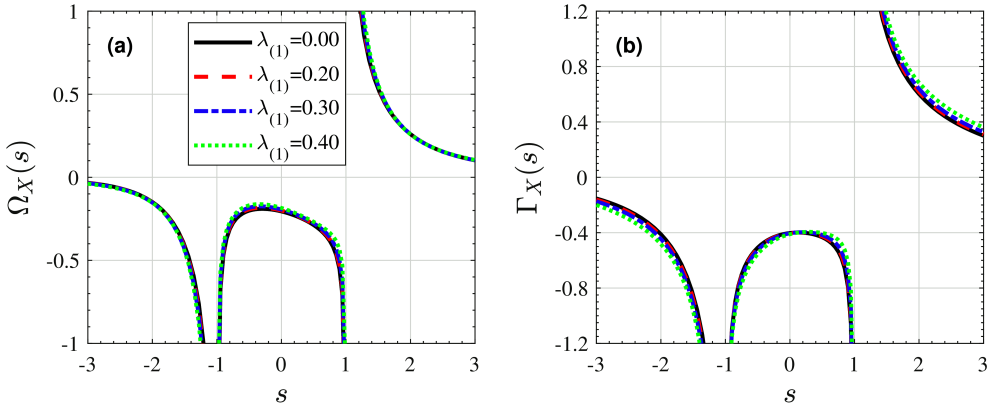


FIG. 6. Normalized electric displacement and magnetic induction as functions of $\lambda_{(1)}$ computed for the FGM2 coating loaded by the moving flat punch: (a) electric displacement; (b) magnetic induction. $h_2/b = 0.5$, $h_3/b = 0.25$, $h_4/b = 0.4375$, $h_c/b = 1$, $\eta = 0.3$.

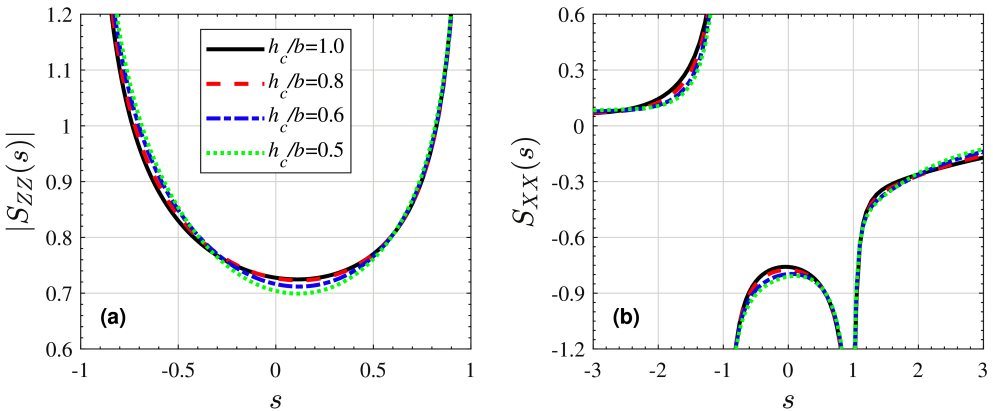


FIG. 7. Normalized contact stresses as functions of h_c/b computed for the FGM2 coating loaded by the moving flat punch: (a) normal stress; (b) normal stress in X-direction. $h_2/b = 0.5$, $h_3/b = 0.25$, $h_4/b = 0.4375$, $\eta = 0.3$, $\lambda_{(1)} = 0.3$.

S_{ZZ} and S_{XX} , tend to become larger as $\lambda_{(1)}$ is increased from 0 to 0.4. Table 5 indicates that mode I stress intensity factors lessen as the dimensionless punch speed increases. Electric displacement and magnetic induction are not that sensitive to the changes in the dimensionless punch speed but for $|s| > 1$ magnitudes of both functions increase as $\lambda_{(1)}$ gets larger. Especially, the elastic response is affected by the punch speed, and a dynamic model based on the wave equations is therefore imperative for accurate analysis.

Another factor that has a bearing on the behavior of the composite medium is the relative thickness of the MEE coating, h_c/b . Figure 7 depicts the influence

TABLE 4. Normalized stress intensity factors computed for different MEE coatings loaded by the moving flat punch. $h_2/b = 0.5$, $h_3/b = 0.25$, $h_4/b = 0.4375$, $h_c/b = 1$, $\eta = 0.3$, $\lambda_{(1)} = 0.3$.

	FGM1	FGM2	FGM3	H
$K_I(-1)$	0.2475	0.2538	0.2664	0.2867
$K_I(1)$	0.2481	0.2577	0.2746	0.2980

TABLE 5. Normalized stress intensity factors computed for different values of $\lambda_{(1)}$ by considering the FGM2 coating in contact with the moving flat punch. $h_2/b = 0.5$, $h_3/b = 0.25$, $h_4/b = 0.4375$, $h_c/b = 1$, $\eta = 0.3$.

	$\lambda_{(1)}$			
	0.00	0.20	0.30	0.40
$K_I(-1)$	0.2699	0.2639	0.2538	0.2305
$K_I(1)$	0.2695	0.2651	0.2577	0.2401

TABLE 6. Normalized stress intensity factors computed for different values of h_c/b by considering the FGM2 coating in contact with the moving flat punch. $h_2/b = 0.5$, $h_3/b = 0.25$, $h_4/b = 0.4375$, $\eta = 0.3$, $\lambda_{(1)} = 0.3$.

	h_c/b			
	0.5	0.6	0.8	1.0
$K_I(-1)$	0.2443	0.2458	0.2496	0.2538
$K_I(1)$	0.2412	0.2443	0.2511	0.2577

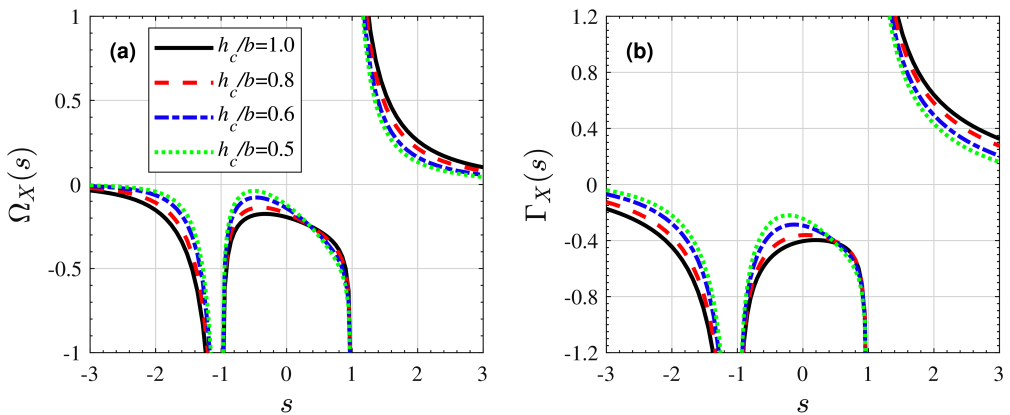


FIG. 8. Normalized electric displacement and magnetic induction as functions of h_c/b computed for the FGM2 coating loaded by the moving flat punch: (a) electric displacement; (b) magnetic induction. $h_2/b = 0.5$, $h_3/b = 0.25$, $h_4/b = 0.4375$, $\eta = 0.3$, $\lambda_{(1)} = 0.3$.

of h_c/b on dimensionless contact stresses in the FGM2 coating. Near the center of the contact zone, $s = 0$, the amplitude of the contact stress, S_{ZZ} , increases whereas that of S_{XX} decreases as h_c/b is increased. Results in Table 6 imply that both of the normalized stress intensity factors are increasing functions of h_c/b . The coupling between the relative thickness and the electromagnetic behavior is found to be significant. Figure 8 shows that outside the contact region, the magnitudes of both electric displacement and magnetic induction become larger with a corresponding increase in the relative thickness.

4.4. Triangular punch

The triangular punch sliding over the MEE multi-layer system is depicted in Fig. 1(b). The pertaining numerical results are provided in Figs. 9–14 and Tables 7–9. Figure 9 examines the effect of the coating type on the contact stresses. The sharp edge of the triangular punch causes a singularity in S_{ZZ} at $s = -1$. At the other end, the contact is smooth, and the normal stress is zero. The contact stress in the lateral direction, S_{XX} , spikes near the trailing end of the contact zone. The contact problem of the triangular punch is incomplete, and as a result contact force P is a function of the contact zone size b . Dimensionless contact force and normalized stress intensity factor at the sharp corner, $s = -1$, are provided in Table 7. Lesser force and SIF values are generated in the homogeneous coating. Among the FGM coatings, lowest magnitudes are calculated for FGM3, for which barium titanate-cobalt ferrite volume fraction is larger throughout the thickness. Normalized electric displacement and magnetic induction in X -direction for different coating types are presented in Fig. 10. Both possess singularities in the neighborhood of the end point, $s = -1$,

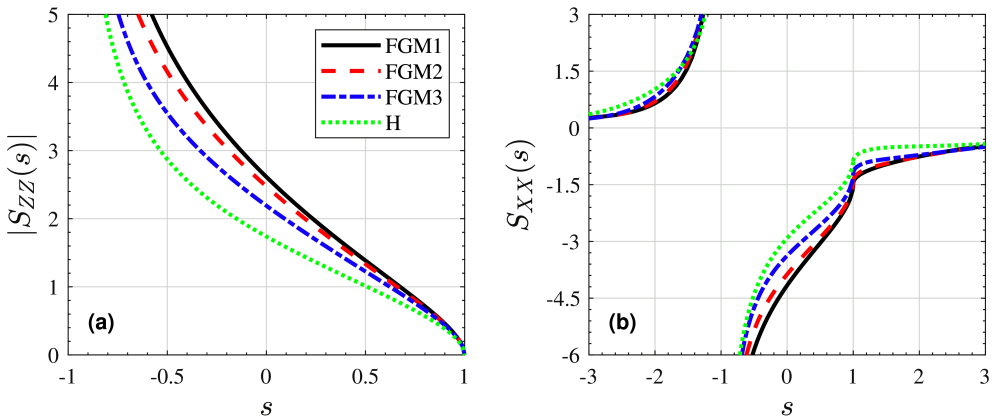


FIG. 9. Normalized contact stresses computed for different MEE coatings loaded by the moving triangular punch: (a) normal stress; (b) normal stress in X -direction. $h_2/b = 0.5$, $h_3/b = 0.25$, $h_4/b = 0.4375$, $h_c/b = 1$, $\eta = 0.3$, $\lambda_{(1)} = 0.3$.

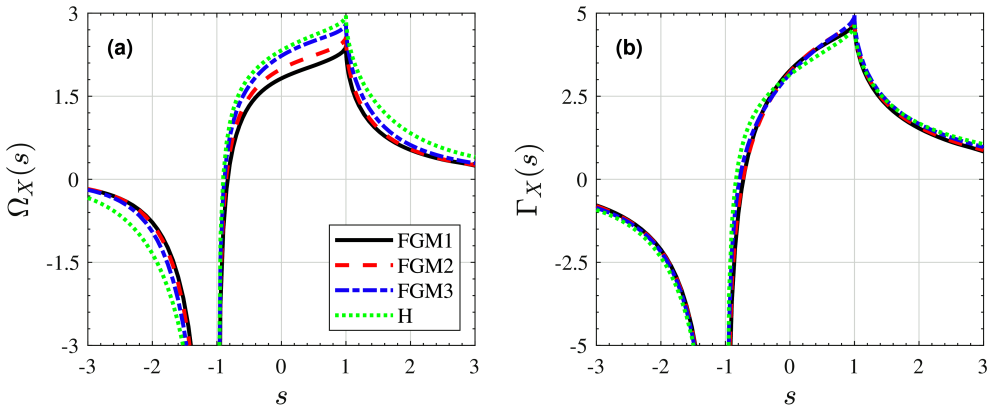


FIG. 10. Normalized electric displacement and magnetic induction computed for different MEE coatings loaded by the moving triangular punch: (a) electric displacement; (b) magnetic induction. $h_2/b = 0.5$, $h_3/b = 0.25$, $h_4/b = 0.4375$, $h_c/b = 1$, $\eta = 0.3$, $\lambda_{(1)} = 0.3$.

TABLE 7. Normalized stress intensity factor and contact force computed for different MEE coatings loaded by the moving triangular punch. $h_2/b = 0.5$, $h_3/b = 0.25$, $h_4/b = 0.4375$, $h_c/b = 1$, $\eta = 0.3$, $\lambda_{(1)} = 0.3$.

	FGM1	FGM2	FGM3	H
$K_I(-1)$	1.7536	1.6754	1.5713	1.4481
$P/(c_{44}(0) \tan(\theta)b)$	3.8019	3.5235	3.1171	2.6415

TABLE 8. Normalized stress intensity factor and contact force computed for different values of $\lambda_{(1)}$ by considering the FGM2 coating in contact with the moving triangular punch. $h_2/b = 0.5$, $h_3/b = 0.25$, $h_4/b = 0.4375$, $h_c/b = 1$, $\eta = 0.3$.

	$\lambda_{(1)}$			
	0.00	0.20	0.30	0.40
$K_I(-1)$	2.0882	1.9142	1.6754	1.2844
$P/(c_{44}(0) \tan(\theta)b)$	4.1003	3.8555	3.5235	2.9932

and go through a maximum at $s = 1$. Largest normalized electric displacement and magnetic induction peaks are calculated, respectively, for the H and FGM3 coatings.

Figures 11 and 12, and Table 8 illustrate the impact of the dimensionless punch speed, $\lambda_{(1)}$, for the coating FGM2. An increase in $\lambda_{(1)}$ lowers the magnitude of S_{ZZ} , as can be seen in Fig. 11(a). Table 8 points out to similar drops in the normalized stress intensity factor and the contact force. Figure 12 shows that electric displacement and magnetic induction peaks at $s = 1$ are affected by the variation in $\lambda_{(1)}$. In both cases, the maximums become smaller as the dimensionless punch speed is increased from 0 to 0.4.

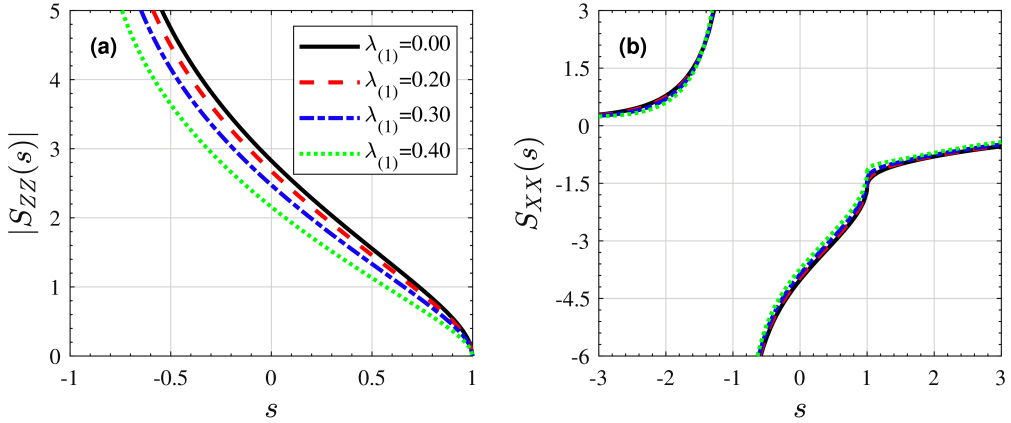


FIG. 11. Normalized contact stresses as functions of $\lambda_{(1)}$ computed for the FGM2 coating loaded by the moving triangular punch: (a) normal stress; (b) normal stress in X -direction. $h_2/b = 0.5, h_3/b = 0.25, h_4/b = 0.4375, h_c/b = 1, \eta = 0.3$.

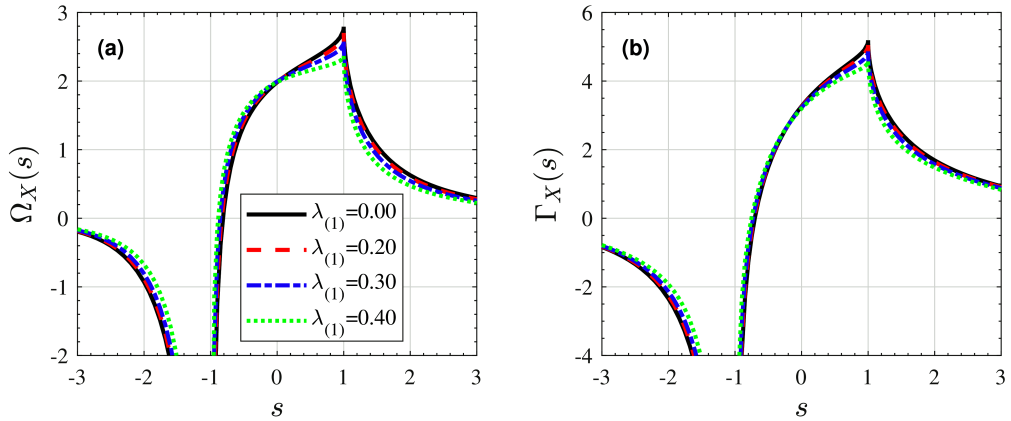


FIG. 12. Normalized electric displacement and magnetic induction as functions of $\lambda_{(1)}$ computed for the FGM2 coating loaded by the moving triangular punch: (a) electric displacement; (b) magnetic induction. $h_2/b = 0.5, h_3/b = 0.25, h_4/b = 0.4375, h_c/b = 1, \eta = 0.3$.

TABLE 9. Normalized stress intensity factor and contact force computed for different values of h_c/b by considering the FGM2 coating in contact with the moving triangular punch. $h_2/b = 0.5, h_3/b = 0.25, h_4/b = 0.4375, \eta = 0.3, \lambda_{(1)} = 0.3$.

	h_c/b			
	0.5	0.6	0.8	1.0
$K_I(-1)$	1.7907	1.7681	1.7200	1.6754
$P/(c_{44}(0) \tan(\theta)b)$	3.9714	3.8862	3.6988	3.5235

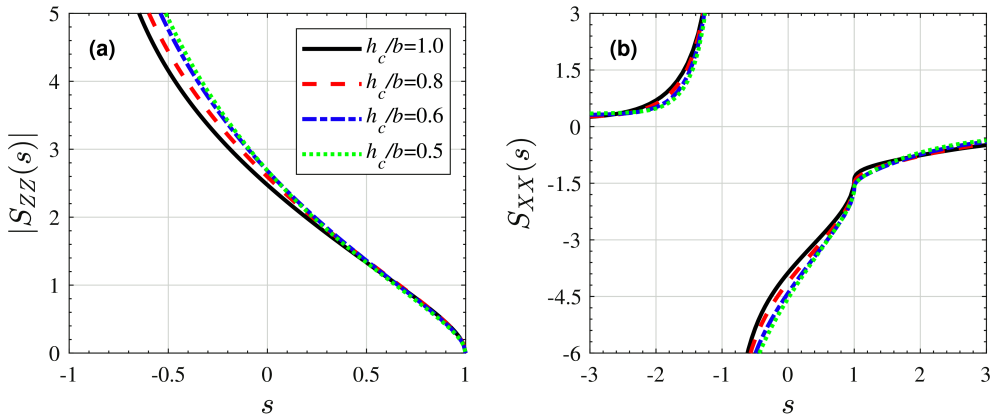


FIG. 13. Normalized contact stresses as functions of h_c/b computed for the FGM2 coating loaded by the moving triangular punch: (a) normal stress; (b) normal stress in X -direction.

$$h_2/b = 0.5, h_3/b = 0.25, h_4/b = 0.4375, \eta = 0.3, \lambda_{(1)} = 0.3.$$

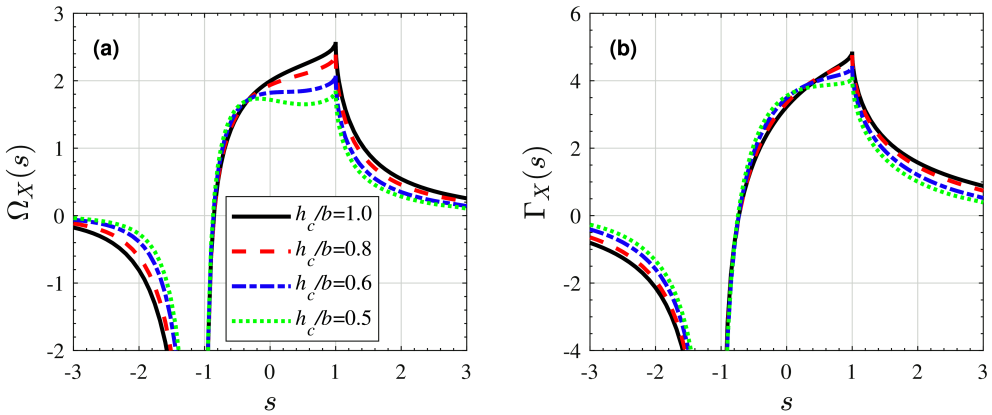


FIG. 14. Normalized electric displacement and magnetic induction as functions of h_c/b computed for the FGM2 coating loaded by the moving triangular punch: (a) electric displacement; (b) magnetic induction. $h_2/b = 0.5, h_3/b = 0.25, h_4/b = 0.4375, \eta = 0.3, \lambda_{(1)} = 0.3.$

The results regarding the influence of relative coating thickness, h_c/b , are presented in Figs. 13 and 14, and Table 9. The computations are carried out for FGM2. Near the sharp end in the contact zone, magnitudes of both S_{ZZ} and S_{XX} tend to lessen with an increase in h_c/b . Stress intensity factor and normalized contact force are also decreasing functions of h_c/b as displayed by Table 9. Electric displacement and magnetic induction plotted in Fig. 14 are both affected by the coating thickness. In particular, the peaks calculated at $s = 1$ and the magnitudes computed for $|s| > 1$ increase as the relative thickness varies from 0.5 to 1.0.

5. Concluding remarks

In this article, we present new solution procedures for moving contact problems of functionally graded multiferroic coatings. A general model involving magneto-electro-elastic layers, elastic interlayers, and an elastic half-plane substrate is constructed. There are a total of four partial differential equations for each MEE layer, whereas two PDE's are to be considered for each of the elastic layers and the half-plane. General solutions are derived by applying Fourier and Galilean transformations. Flat and triangular punch profiles are considered, and the problem is eventually reduced to a singular integral equation in both cases. An expansion-collocation technique is introduced to numerically solve the integral equations. Numerical results illustrate contact stresses, electric displacement, magnetic induction, stress intensity factors, and required contact force as functions of the problem parameters.

The distinguishing feature of the solution procedure for moving contact problems is the consideration of elastic wave equations in the formulation. Resulting analytical framework allows inclusion of the punch velocity in the analysis of the magneto-electro-elastic response. This effect is studied for two different punch profiles, which result in fundamentally different stress distributions in the contact zone. This is due to the fact that there are two points of singularity in the case of the flat punch, whereas the triangular punch causes singularity at only the trailing end. The strengths of singularity are quantified by the stress intensity factors, which are shown to be dependent upon the punch velocity. Thus, application of elastodynamic theory and wave equations is required for accurate assessment of magneto-electro-elastic response under moving contact conditions.

In the multi-layer technique proposed, smooth spatial variations are accounted for by considering a sufficiently large number of layers and calculating the properties at the centroids. As a consequence, functional form for each property of the FGM MEE coating can be prescribed separately in the computations. For both flat and triangular punches, the parametric analyses point out to a strong correlation between the FGM coating type and the response of the MEE system. Electromagnetism displayed is also shown to be influenced by the elastic coating thickness. Hence, modelling of independent property gradations and development of a coupled multi-physics formulation are both imperative for reliable prediction of the behavior of magneto-electro-elastic materials.

Our findings indicate that stress intensity factors calculated at the end points of the flat punch for a homogeneous MEE coating are greater than those evaluated for FGM MEE coatings. Thus, in the presence of singularities at both ends, introduction of gradation into the coating could lead to lower end-point stresses and stress intensity factors. Outside the contact zone of the flat punch, larger magneto-electric magnitudes are also obtained for the homogeneous coat-

ing. The influence of punch speed is analyzed by considering the coating FGM2. In the central region of the contact zone, $|S_{ZZ}(s)|$ induced by the flat punch becomes larger with a corresponding increase in punch velocity. For the triangular punch however, the dimensionless magnitude decreases as the punch velocity is increased. Parametric analyses conducted to examine the impact of relative coating thickness indicate that, in the vicinity of the mid-point of the contact zone, smallest h_c/b leads to lower $|S_{ZZ}|$ values for a flat punch. This trend seems to be again reversed in the case of the triangular punch, for which larger h_c/b causes smaller magnitude.

The methods we present are general in that they account for a wide range of parameters and variables including numbers of magneto-electro-elastic layers and elastic interlayers, nonproportional material property variation functions, speed of the sliding punch, coefficient of kinetic friction, and coating thickness. Computation of results with high accuracy requires the consideration of these factors in the analytical formulation. The solution procedures detailed could therefore prove useful in mechanical design and optimization of functionally graded multiferroics that are under the effect of moving contact loading.

Acknowledgements

This work was supported by the Scientific and Technological Research Council of Turkey (TÜBİTAK) through grant 122M784. Selim E. Toktaş gratefully acknowledges the financial support of TÜBİTAK through BİDEB 2211 A program and scholarship number 1649B032100684.

Appendix: Integrand functions of the Fredholm kernels and constants

The Fredholm kernels of the singular integral equation are defined by Eq. (2.21). The integrand functions in these improper integrals are expressed as follows:

$$(A.1) \quad h_{11}(\zeta) = \text{coeff} \left(\left(\begin{array}{l} G_{(N+M+1)(1)} F_{(N+M+1)(1)} e^{s(N+M+1)(1)Z} + G_{(N+M+1)(2)} F_{(N+M+1)(2)} e^{s(N+M+1)(2)Z} \\ + G_{(N+M+1)(3)} F_{(N+M+1)(3)} e^{s(N+M+1)(3)Z} + G_{(N+M+1)(4)} F_{(N+M+1)(4)} e^{s(N+M+1)(4)Z} \\ + G_{(N+M+1)(5)} F_{(N+M+1)(5)} e^{s(N+M+1)(5)Z} + G_{(N+M+1)(6)} F_{(N+M+1)(6)} e^{s(N+M+1)(6)Z} \\ + G_{(N+M+1)(7)} F_{(N+M+1)(7)} e^{s(N+M+1)(7)Z} + G_{(N+M+1)(8)} F_{(N+M+1)(8)} e^{s(N+M+1)(8)Z} \end{array} \right), P \right),$$

$$(A.2) \quad h_{12}(\zeta) = \text{coeff} \left(\left(\begin{array}{l} G_{(N+M+1)(1)} F_{(N+M+1)(1)} e^{s(N+M+1)(1)Z} + G_{(N+M+1)(2)} F_{(N+M+1)(2)} e^{s(N+M+1)(2)Z} \\ + G_{(N+M+1)(3)} F_{(N+M+1)(3)} e^{s(N+M+1)(3)Z} + G_{(N+M+1)(4)} F_{(N+M+1)(4)} e^{s(N+M+1)(4)Z} \\ + G_{(N+M+1)(5)} F_{(N+M+1)(5)} e^{s(N+M+1)(5)Z} + G_{(N+M+1)(6)} F_{(N+M+1)(6)} e^{s(N+M+1)(6)Z} \\ + G_{(N+M+1)(7)} F_{(N+M+1)(7)} e^{s(N+M+1)(7)Z} + G_{(N+M+1)(8)} F_{(N+M+1)(8)} e^{s(N+M+1)(8)Z} \end{array} \right), Q \right),$$

$$(A.3) \quad h_{21}(\zeta) = \text{coeff} \left(\left(\begin{array}{l} G_{(N+M+1)(1)} e^{s(N+M+1)(1)Z} + G_{(N+M+1)(2)} e^{s(N+M+1)(2)Z} + G_{(N+M+1)(3)} e^{s(N+M+1)(3)Z} \\ + G_{(N+M+1)(4)} e^{s(N+M+1)(4)Z} + G_{(N+M+1)(5)} e^{s(N+M+1)(5)Z} + G_{(N+M+1)(6)} e^{s(N+M+1)(6)Z} \\ + G_{(N+M+1)(7)} e^{s(N+M+1)(7)Z} + G_{(N+M+1)(8)} e^{s(N+M+1)(8)Z} \end{array} \right), Q \right),$$

$$(A.4) \quad h_{22}(\zeta) = \text{coeff} \left(\left(\begin{array}{l} G_{(N+M+1)(1)} e^{s(N+M+1)(1)Z} + G_{(N+M+1)(2)} e^{s(N+M+1)(2)Z} + G_{(N+M+1)(3)} e^{s(N+M+1)(3)Z} \\ + G_{(N+M+1)(4)} e^{s(N+M+1)(4)Z} + G_{(N+M+1)(5)} e^{s(N+M+1)(5)Z} + G_{(N+M+1)(6)} e^{s(N+M+1)(6)Z} \\ + G_{(N+M+1)(7)} e^{s(N+M+1)(7)Z} + G_{(N+M+1)(8)} e^{s(N+M+1)(8)Z} \end{array} \right), P \right),$$

$$(A.5) \quad h_{31}(\zeta) = \text{coeff} \left(\left(\begin{array}{l} G_{(N+M+1)(1)} R_{(N+M+1)(1)} e^{s(N+M+1)(1)Z} + G_{(N+M+1)(2)} R_{(N+M+1)(2)} e^{s(N+M+1)(2)Z} \\ + G_{(N+M+1)(3)} R_{(N+M+1)(3)} e^{s(N+M+1)(3)Z} + G_{(N+M+1)(4)} R_{(N+M+1)(4)} e^{s(N+M+1)(4)Z} \\ + G_{(N+M+1)(5)} R_{(N+M+1)(5)} e^{s(N+M+1)(5)Z} + G_{(N+M+1)(6)} R_{(N+M+1)(6)} e^{s(N+M+1)(6)Z} \\ + G_{(N+M+1)(7)} R_{(N+M+1)(7)} e^{s(N+M+1)(7)Z} + G_{(N+M+1)(8)} R_{(N+M+1)(8)} e^{s(N+M+1)(8)Z} \end{array} \right), P \right),$$

$$(A.6) \quad h_{32}(\zeta) = \text{coeff} \left(\left(\begin{array}{l} G_{(N+M+1)(1)} R_{(N+M+1)(1)} e^{s(N+M+1)(1)Z} + G_{(N+M+1)(2)} R_{(N+M+1)(2)} e^{s(N+M+1)(2)Z} \\ + G_{(N+M+1)(3)} R_{(N+M+1)(3)} e^{s(N+M+1)(3)Z} + G_{(N+M+1)(4)} R_{(N+M+1)(4)} e^{s(N+M+1)(4)Z} \\ + G_{(N+M+1)(5)} R_{(N+M+1)(5)} e^{s(N+M+1)(5)Z} + G_{(N+M+1)(6)} R_{(N+M+1)(6)} e^{s(N+M+1)(6)Z} \\ + G_{(N+M+1)(7)} R_{(N+M+1)(7)} e^{s(N+M+1)(7)Z} + G_{(N+M+1)(8)} R_{(N+M+1)(8)} e^{s(N+M+1)(8)Z} \end{array} \right), Q \right),$$

$$(A.7) \quad h_{41}(\zeta) = \text{coeff} \left(\left(\begin{array}{l} G_{(N+M+1)(1)} Y_{(N+M+1)(1)} e^{s(N+M+1)(1)Z} + G_{(N+M+1)(2)} Y_{(N+M+1)(2)} e^{s(N+M+1)(2)Z} \\ + G_{(N+M+1)(3)} Y_{(N+M+1)(3)} e^{s(N+M+1)(3)Z} + G_{(N+M+1)(4)} Y_{(N+M+1)(4)} e^{s(N+M+1)(4)Z} \\ + G_{(N+M+1)(5)} Y_{(N+M+1)(5)} e^{s(N+M+1)(5)Z} + G_{(N+M+1)(6)} Y_{(N+M+1)(6)} e^{s(N+M+1)(6)Z} \\ + G_{(N+M+1)(7)} Y_{(N+M+1)(7)} e^{s(N+M+1)(7)Z} + G_{(N+M+1)(8)} Y_{(N+M+1)(8)} e^{s(N+M+1)(8)Z} \end{array} \right), P \right),$$

$$(A.8) \quad h_{42}(\zeta) = \text{coeff} \left(\left(\begin{array}{l} G_{(N+M+1)(1)} Y_{(N+M+1)(1)} e^{s(N+M+1)(1)Z} + G_{(N+M+1)(2)} Y_{(N+M+1)(2)} e^{s(N+M+1)(2)Z} \\ + G_{(N+M+1)(3)} Y_{(N+M+1)(3)} e^{s(N+M+1)(3)Z} + G_{(N+M+1)(4)} Y_{(N+M+1)(4)} e^{s(N+M+1)(4)Z} \\ + G_{(N+M+1)(5)} Y_{(N+M+1)(5)} e^{s(N+M+1)(5)Z} + G_{(N+M+1)(6)} Y_{(N+M+1)(6)} e^{s(N+M+1)(6)Z} \\ + G_{(N+M+1)(7)} Y_{(N+M+1)(7)} e^{s(N+M+1)(7)Z} + G_{(N+M+1)(8)} Y_{(N+M+1)(8)} e^{s(N+M+1)(8)Z} \end{array} \right), Q \right),$$

where $\text{coeff}(\cdot, \cdot)$ stands for the coefficient of the parameter following comma in the entire expression in parentheses; and P and Q are, respectively, normal and tangential forces transferred by the contact.

The constants used in Eqs. (2.20), (3.11), and (3.19) are of the forms

$$(A.9) \quad p_9 = c_{(N+M+1)13} \Delta_{111} + e_{(N+M+1)31} \Delta_{121} + f_{(N+M+1)31} \Delta_{131},$$

$$(A.10) \quad p_{10} = c_{(N+M+1)11} - c_{(N+M+1)13} \Delta_{21} - e_{(N+M+1)31} \Delta_{22} - f_{(N+M+1)31} \Delta_{23},$$

$$(A.11) \quad p_{11} = \frac{e_{(N+M+1)15}}{c_{(N+M+1)44}}, \quad p_{12} = \frac{e_{(N+M+1)15}^2}{c_{(N+M+1)44}} + \beta_{(N+M+1)11},$$

$$p_{13} = \frac{e_{(N+M+1)15} f_{(N+M+1)15}}{c_{(N+M+1)44}} + g_{(N+M+1)11},$$

$$(A.12) \quad p_{14} = \frac{f_{(N+M+1)15}}{c_{(N+M+1)44}}, \quad p_{15} = \frac{f_{(N+M+1)15}^2}{c_{(N+M+1)44}} + \mu_{(N+M+1)11},$$

$$p_{16} = \frac{c_{33}(0)}{e_{33}(0)}, \quad p_{17} = \frac{c_{33}(0)}{f_{33}(0)},$$

$$(A.13) \quad \begin{bmatrix} \Delta_{111} & \Delta_{112} & \Delta_{113} \\ \Delta_{121} & \Delta_{122} & \Delta_{123} \\ \Delta_{131} & \Delta_{132} & \Delta_{133} \end{bmatrix} = \begin{bmatrix} c_{(N+M+1)33} & e_{(N+M+1)33} & f_{(N+M+1)33} \\ e_{(N+M+1)33} & -\beta_{(N+M+1)33} & -g_{(N+M+1)33} \\ f_{(N+M+1)33} & -g_{(N+M+1)33} & -\mu_{(N+M+1)33} \end{bmatrix}^{-1},$$

$$(A.14) \quad \left\{ \begin{array}{l} \Delta_{21} \\ \Delta_{22} \\ \Delta_{23} \end{array} \right\} = \begin{bmatrix} c_{(N+M+1)33} & e_{(N+M+1)33} & f_{(N+M+1)33} \\ e_{(N+M+1)33} & -\beta_{(N+M+1)33} & -g_{(N+M+1)33} \\ f_{(N+M+1)33} & -g_{(N+M+1)33} & -\mu_{(N+M+1)33} \end{bmatrix}^{-1} \left\{ \begin{array}{l} c_{(N+M+1)13} \\ e_{(N+M+1)31} \\ f_{(N+M+1)31} \end{array} \right\}.$$

References

1. C. DONG, X. LIANG, J. GAO, H. CHEN, Y. HE, Y. WEI, M. ZAEIMBASHI, A. MATYUSHOV, C. SUN, N.X. SUN, *Thin film magnetoelectric sensors toward biomagnetism: materials, devices, and applications*, *Advanced Electronic Materials*, **8**, 2200013, 2022.
2. B. BEHERA, B.C. SUTAR, N.R. PRADHAN, *Recent progress on 2D ferroelectric and multiferroic materials, challenges, and opportunity*, *Emergent Materials*, **4**, 847–863, 2021.
3. K. MALLERON, A. GENSBITTEL, H. TALLEB, Z. REN, *Experimental study of magnetoelectric transducers for power supply of small biomedical devices*, *Microelectronics Journal*, **88**, 184–189, 2019.
4. Y. WANG, J. LI, D. VIEHLAND, *Magnetoelectrics for magnetic sensor applications: status, challenges, and perspectives*, *Materials Today*, **17**, 269–275, 2014.
5. J. MA, J. HU, Z. LI, C.-W. NAN, *Recent progress in multiferroic magnetoelectric composites: from bulk to thin films*, *Advanced Materials*, **23**, 1062–1087, 2011.
6. Z. SUROWIAK, D. BOCHENEK, *Multiferroic materials for sensors, transducers, and memory devices*, *Archives of Acoustics*, **33**, 243–260, 2008.
7. V. BOGGARAPU, R. GUJJALA, S. OJHA, S. ACHARYA, P. VENKATESWARA BABU, S. CHOWDARY, D.K. GARA, *State of the art in functionally graded materials*, *Composite Structures*, **262**, 113596, 2021.
8. P. HAJHEIDARI, I. STIHARU, R. BHAT, *Performance of non-uniform functionally graded piezoelectric energy harvester beams*, *Journal of Intelligent Material Systems and Structures*, **31**, 1604–1616, 2020.
9. B. SALEH, J. JIANG, R. FATHI, T. AL-HABABI, Q. XU, L. WANG, D. SONG, A. MA, *30 years of functionally graded materials: an overview of manufacturing methods, applications and future challenges*, *Composites Part B: Engineering*, 201, 108376, 2020.

10. S. VIJAYAVENKATARAMAN, L.Y. KUAN, W.F. LU, *3D-printed ceramic triply periodic minimal surface structures for design of functionally graded bone implants*, *Materials & Design*, **191**, 108602, 2020.
11. S. KUMAR, K.V.V.S. MURTHY REDDY, A. KUMAR, G. ROHINI DEVI, *Development and characterization of polymer-ceramic fiber-reinforced functionally graded composites for aerospace application*, *Aerospace Science and Technology*, **26**, 185–191, 2013.
12. S.E. TOKTAŞ, S. DAG, *Multi-layer model for moving contact problems of functionally graded coatings with general variations in physical properties*, *Proceedings of the Institution of Mechanical Engineers, Part L: Journal of Materials: Design and Applications*, **236**, 1967–1980, 2022.
13. S.E. TOKTAŞ, S. DAG, *Stresses in multi-layer coatings in Hertzian contact with a moving circular punch*, *Tribology International*, **171**, 107565, 2022.
14. I. ESHRAGHI, S. DAG, *Transient dynamic analysis of functionally graded micro-beams considering small-scale effects*, *Archives of Mechanics*, **73**, 303–337, 2021.
15. F.P.E. NGAİK, G.E. NTAMACK, L. AZRAR, *Three dimensional modeling of static deformation of arbitrary functionally graded multilayered multiferroic composite plates with weakly and highly conducting imperfect interfaces*, *Journal of Intelligent Material Systems and Structures*, **32**, 2066–2091, 2021.
16. J. YAN, C. MI, *Double contact analysis of multilayered elastic structures involving functionally graded materials*, *Archives of Mechanics*, **69**, 199–221, 2017.
17. R. WANG, E. PAN, *Three-dimensional modeling of functionally graded multiferroic composites*, *Mechanics of Advanced Materials and Structures*, **18**, 68–76, 2011.
18. W. CHEN, E. PAN, H. WANG, C. ZHANG, *Theory of indentation on multiferroic composite materials*, *Journal of the Mechanics and Physics of Solids*, **58**, 1524–1551, 2010.
19. J. MA, L.-L. KE, Y.-S. WANG, *Frictionless contact of a functionally graded magneto-electro-elastic layered half-plane under a conducting punch*, *International Journal of Solids and Structures*, **51**, 2791–2806, 2014.
20. R. ELLOUMI, I. KALLEL-KAMOUN, S. EL-BORGI, M.A. GULER, *Closed-form solutions of the frictional sliding contact problem for a magneto-electro-elastic half-plane indented by rigid conducting punch*, *International Journal of Solids and Structures*, **50**, 3778–3792, 2013.
21. R. ELLOUMI, I. KALLEL-KAMOUN, S. EL-BORGI, M.A. GULER, *On the frictional sliding contact problem between a rigid circular conducting punch and a magneto-electro-elastic half-plane*, *International Journal of Mechanical Sciences*, **87**, 1–17, 2014.
22. Y.-T. ZHOU, T.-W. KIM, *An exact analysis of sliding frictional contact of a rigid punch over the surface of magneto-electro-elastic materials*, *Acta Mechanica*, **225**, 625–645, 2014.
23. Y.-T. ZHOU, K.Y. LEE, *Theory of sliding contact for multiferroic materials indented by a rigid punch*, *International Journal of Mechanical Sciences*, **66**, 156–167, 2013.
24. R. ELLOUMI, S. EL-BORGI, M.A. GULER, I. KALLEL-KAMOUN, *The contact problem of a rigid stamp with friction on a functionally graded magneto-electro-elastic half-plane*, *Acta Mechanica*, **227**, 1123–1156, 2016.
25. J. MA, L.-L. KE, Y.-S. WANG, *Sliding frictional contact of functionally graded magneto-electro-elastic materials under a conducting flat punch*, *Journal of Applied Mechanics – Transactions of the ASME*, **82**, 011009-1, 2015.

26. X. ZHANG, Z. WANG, H. SHEN, Q.J. WANG, *Frictional contact involving a multiferroic thin film subjected to surface magneto-electroelastic effects*, International Journal of Mechanical Sciences, **131–132**, 633–648, 2017.
27. H. ZHANG, W. WANG, Y. LIU, Z. ZHAO, *Semi-analytic modelling of transversely isotropic magneto-electro-elastic materials under frictional sliding contact*, Applied Mathematical Modelling, **75**, 116–140, 2019.
28. I. ÇÖMEZ, *Thermoelastic contact problem of a magneto-electro-elastic layer indented by a rigid insulating punch*, Mechanics of Advanced Materials and Structures, **29**, 7231–7245, 2022.
29. J. MA, S. EL-BORGI, L.-L. KE, Y.-S. WANG, *Frictional contact problem between a functionally graded magneto-electroelastic layer and a rigid conducting flat punch with frictional heat generation*, Journal of Thermal Stresses, **39**, 245–277, 2016.
30. I. ÇÖMEZ, *Frictional moving contact problem of a magneto-electro-elastic half plane*, Mechanics of Materials, **154**, 103704, 2021.
31. Y.-T. ZHOU, K.Y. LEE, *Contact problem for magneto-electro-elastic half-plane materials indented by a moving punch. Part I: Closed-form solutions*, International Journal of Solids and Structures, **49**, 3853–3865, 2012.
32. Y.-T. ZHOU, K.Y. LEE, *Contact problem for magneto-electro-elastic half-plane materials indented by a moving punch. Part II: Numerical results*, International Journal of Solids and Structures, **49**, 3866–3882, 2012.
33. Y. MEI, Z. DUAN, Z. LI, Y. ZHAO, J. NI, Y. LI, J. ZHANG, Y. CHEN, X. WANG, G. ZHAO, *Enhanced multiferroic properties of $Bi_4Ti_{3-x}Co_xO_{12}/La_{0.67}Sr_{0.33}MnO_3$ layered composite thin films*, Ceramics International, **48**, 21728–21738, 2022.
34. M. SCIGAJ, N. DIX, J. GAZQUEZ, M. VARELA, I. FINA, N. DOMINGO, G. HER-RANZ, V. SKUMRYEV, J. FONTCUBERTA, F. SANCHEZ, *Monolithic integration of room-temperature multifunctional $BaTiO_3$ - $CoFe_2O_4$ epitaxial heterostructures on $Si(001)$* , Scientific Reports, **6**, 31870, 2016.
35. S. SHARMA, M. TOMAR, A. KUMAR, N.K. PURI, V. GUPTA, *Multiferroic properties of $BiFeO_3/BaTiO_3$ multilayered thin films*, Physica B: Condensed Matter, **448**, 125–127, 2014.
36. X. WANG, E. PAN, J.D. ALBRECHT, W.J. FENG, *Effective properties of functionally graded multiferroic composites*, Composite Structures, **87**, 206–214, 2009.
37. S. DAG, *Crack and Contact Problems in Graded Materials*, Ph.D. Dissertation, Lehigh University, Bethlehem, PA, USA, 2001.
38. MEMSnet, *Material: silicon (Si), bulk*, [online], available at: <https://www.memsnet.org/material/siliconsibulk/> (accessed 14 July 2023).
39. K. SUZUKI, M. KATO, T. SUNAOSHI, H. UNO, U. CARVAJAL-NUNEZ, A.T. NELSON, K.J. MCCLELLAN, *Thermal and mechanical properties of CeO_2* , Journal of the American Ceramic Society, **102**, 1994–2008, 2019.
40. A.R. ANNAMALAI, N. NAGARAJU, D.K. AGRAWAL, A. MUTHUCHAMY, *Effect of heating mode on sinterability of $YSZ+CeO_2$ ceramics*, Metals, **8**, 1–7, 2018.
41. M. GOLALIKHANI, Q. LEI, R.U. CHANDRASENA, L. KASAEI, H. PARK, J. BAI, P. ORGIANI, CISTON, G.E. STERBINSKY, D.A. ARENA, P. SHAFER, E. ARENHOLZ,

B.A. DAVIDSON, A.J. MILLIS, A.X. GRAY, X.X. XI, *Nature of the metal-insulator transition in few-unit-cell-thick LaNiO₃ films*, Nature Communications, **9**, 1–8, 2018.

42. S. MASYS, V. JONAUSKAS, *Elastic properties of rhombohedral, cubic, and monoclinic phases of LaNiO₃ by first principles calculations*, Computational Materials Science, **108**, 153–159, 2015.
43. S. GIRAUD, J. CANEL, *Young's modulus of some SOFCs materials as a function of temperature*, Journal of the European Ceramic Society, **28**, 77–83, 2008.

Received March 20, 2023; revised version June 12, 2023.

Published online September 5, 2023.
